We are IntechOpen, the world's leading publisher of Open Access books Built by scientists, for scientists

6,900
Open access books available

186,000
International authors and editors

200M
Downloads

Our authors are among the

154
Countries delivered to

TOP 1%
most cited scientists

12.2%
Contributors from top 500 universities

WEB OF SCIENCE™

Selection of our books indexed in the Book Citation Index in Web of Science™ Core Collection (BKCI)

Interested in publishing with us?
Contact book.department@intechopen.com

Numbers displayed above are based on latest data collected.
For more information visit www.intechopen.com

Chapter 5

Azodendrimers as a Functional Material

Hideo Takezoe and Osamu Haba

Additional information is available at the end of the chapter

http://dx.doi.org/10.5772/intechopen.70715

Abstract

Dendrimers can behave as active functional materials, if they are substituted at their tail ends by azo groups. The dendrimers we developed spontaneously attach to interfaces or surfaces, providing us with a variety of functions. After describing the synthesis of dendrimers and azodendrimers, we first review functions for static uses; alignment surface for liquid crystals (LCs). Then, a major part of this review is devoted to the introduction for dynamic uses. Because of photo-induced *trans-cis* isomerization, the azodendrimers act as a command surface, which enables us to control LC orientation. Azodendrimer layers were formed at glass substrates, LC droplets in polymers, and surfaces of microparticles in LCs. Photo-controlled *trans*- and *cis*-forms, respectively, provide homeotropic and planar orientations of LCs. The photo-irradiation induces dewetting of dendrimer layers as well. Photo-induced orientation changes of LCs provide us with various applications and novel phenomena; photo-controlled macroscopic physical properties such as thermal transport, defect structure changes in LC colloids and LC systems with microinclusions, and even dynamics of inclusions in LCs.

Keywords: azo, surface, interface, liquid crystal, command surface, photo-induced phenomenon, dewetting, liquid crystal colloid, microparticle, defect structure

1. Introduction

Azo molecules show photo-induced conformational changes based on *trans-cis* photo-isomerization. The conformational changes lead to various functions such as a macroscopic deformation in polymers containing azo groups [1] and a command surface for liquid crystals (LCs) providing orientation changes [2, 3]. The readers may find a lot of review articles on this topic [4]. Dendrimers have a controlled structure with a central core and well-defined branched terminals and have been an expanding research area in recent three decades [5]. We can easily imagine that dendrimers with azo chromophores (azodendrimers) in the internal structure and on peripheries are quite intriguing research aspects in material

IntechOpen

© 2018 The Author(s). Licensee IntechOpen. This chapter is distributed under the terms of the Creative Commons Attribution License (http://creativecommons.org/licenses/by/3.0), which permits unrestricted use, distribution, and reproduction in any medium, provided the original work is properly cited. CC BY

science and applications. Namely, photo-irradiation onto azodendrimers exerts not only the *trans-cis* conformational change of azo moiety but also the dendrimer structure, which brings about a variety of functions [6]; switching device or data storage using Langmuir-Blodgett films of azodendrimer molecules [7], active materials for electro-optic applications [8], LC photo-orientation [9], photo-controlled chirooptics [10], and enhanced optical nonlinearity [11]. We found some additional benefits by introducing azo linkages into our dendrimers. In this chapter, we review such functions offered by azobenzene-containing dendrimers (azodendrimers). After an introduction and syntheses of azodendrimers, we describe (1) spontaneous surface modification by dendrimers for LC displays, (2) application for controlling physical parameters, (3) photo-triggered dewetting surface and its control, (4) application to memory devices using a LC showing an anchoring transition, (5) command surfaces in restricted surfaces such as LC droplets, silica microparticle surfaces, and (6) controlling surface anchoring strength for LC orientation. Through these applications, we want to emphasize the important functions, which are provided not only by dendrimers themselves but also by introducing azo groups into dendrimers.

2. Motivation and synthesis

Dendrimers are a kind of polymeric materials consisting of regular multi-branched structure with a specific topology. Dendrimers are known to exhibit low viscosity and good solubility comparing with linear polymers with comparable molecular weights because of less tangled molecular structures. Their molecular structures consist of core units, branched repeating units, and terminal groups. The modifications of the terminals are quite easy because the terminal functional groups are not hindered unlike the functional groups bound to the crowding main chain of linear polymers.

Introducing mesogenic groups into the terminal groups of flexible dendrimers provides the dendrimers with liquid crystalline natures [12]. Then we can expect better compatibility of the dendrimer with LCs. Such liquid crystalline dendrimers can be prepared using commercial polypropyleneimine dendrimers (PPIDs), whose chemical structure is shown in **Figure 1(a)**, and mesogen-carrying acrylates through the double-Michael addition to produce tertiary amine linkages, as shown in **Figure 1(b)** [13]. For the latter, we can use numerous acrylates, which have been reported in many literatures, developed for the syntheses of side-chain liquid crystalline polymers. The reaction can be carried out by simply heating in THF solution at 40–50°C, but requires two or more weeks in order to prevent the reaction from stopping at the secondary amine stage, which is difficult to be removed from the final product. Once the complete Michael addition, which means the absence of the residual primary or secondary amines, can be achieved, the resulting liquid crystalline dendrimer can be purified by simple precipitation to poor solvents such as methanol or hexane, which is chosen based on the solubility of the mesogenic units.

We have introduced various mesogens including biphenyls, phenyl benzoates, cyclohexylbenzene, and azobenzenes, as shown in **Figure 2** [13, 14]. We refer the liquid crystalline dendrimers as D*G*-*n*X, where *G* is the generation of PPID, *n* is the number of carbon atoms of the alkylene spacer between PPID and the mesogenic unit, and X represents the mesogen. The

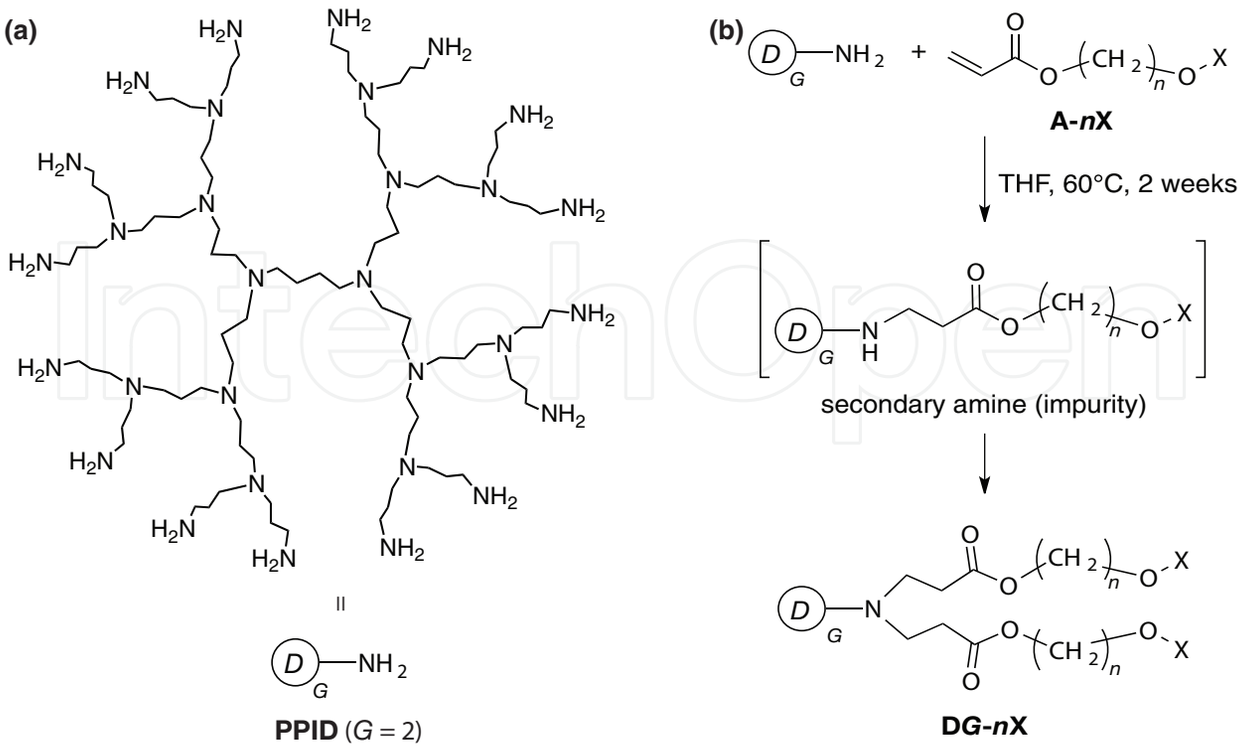

Figure 1. (a) Chemical structure of a polypropyleneimine dendrimers (PPID). *G* indicates the generation of PPID. (b) Preparation scheme of a liquid crystalline dendrimer from PPID and a mesogen-carrying acrylate. For X, see **Figure 2**.

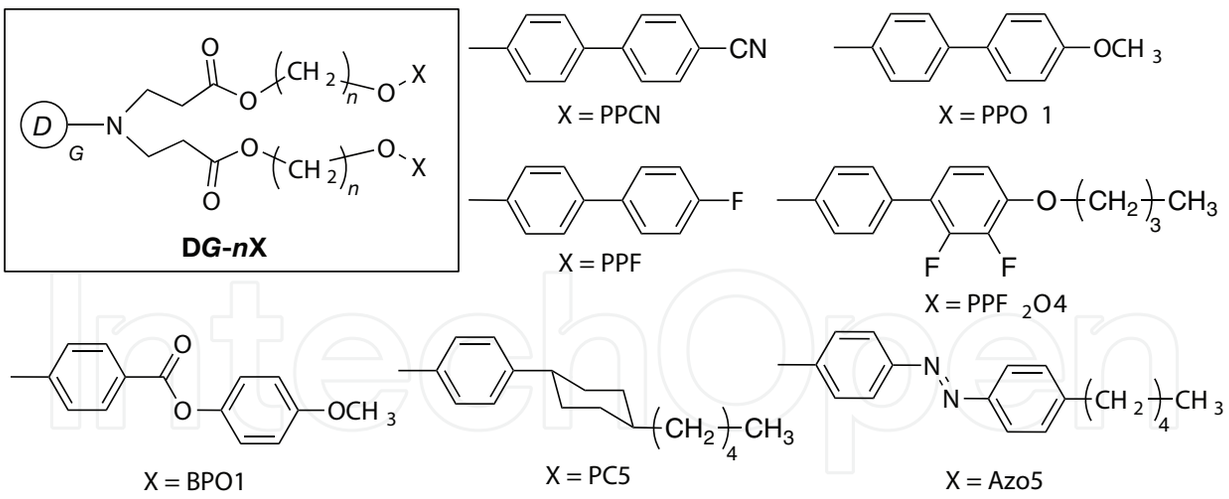

Figure 2. Chemical structures of mesogenic groups used for the preparation of liquid crystalline dendrimers synthesized. Please refer to **Table 1** for the phase sequences of each molecule.

obtained dendrimers exhibited thermotropic liquid crystalline nature. The phase transition temperatures are shown in **Table 1**. Regardless of the mesogen structure, the dendrimers tend to exhibit smectic (Sm) liquid crystalline phases. In the D*G*-10PPF$_2$O4 series, the larger generations of PPID made the smectic-isotropic transition temperature higher, but the generation

Dendrimer	Phase transition temperature[a]/°C	Homeotropic alignment[d]
D2-6PPCN	I 68 SmA −5 G	+
D2-6PPO1	I 96 SmA 90 SmE[b]	−
D2-6PPF	I 50 SmE[b]	−
D1-10PPF$_2$O4	I 72 SmA 56 SmE[b]	−
D2-10PPF$_2$O4	I 78 SmA 58 SmE[b]	+
D3-10PPF$_2$O4	I 86 SmA 51 SmE[b]	+
D4-10PPF$_2$O4	I 91 SmA 54 SmE[b]	+
D5-10PPF$_2$O4	I 97 SmA 54 SmE[b]	−
D2-6BPO1	I 67 SmA −3 G	−
D2-3PC5	I 74 SmA 16 SmB −14 G	+
D2-6PC5	I 69 SmA 17 SmB −21 G	+
D2-12PC5	I 80 SmA 73 SmB 5 G	−
D2-6Azo5	G − 5 SmB 34 SmA 85 I[c]	+

Signs: +, exhibited homeotropic orientation; −, exhibited random orientation.
[a]Recorded during the 2nd cooling scan with $\Delta T = -10$°C/min.
[b]Glass transition temperatures were not observed above −20°C.
[c]Recorded during the heating scan ($\Delta T = 10$°C/min).
[d]Tendency to show spontaneous homeotropic alignment between glass plates on slow cooling.

Table 1. The phase transition temperatures and the homeotropic alignment capability of the liquid crystalline dendrimers.

(*G*) did not affect the liquid crystalline phase. In the D2-*n*PC5 series, the longer alkylene spacers tend to stabilize the SmB phase rather than the SmA phase, which influences the spontaneous alignment of the dendrimers in cells, as will be mentioned below.

Some dendrimers exhibit spontaneous homeotropic orientation between two bare glass surfaces on slow cooling (typically $\Delta T = -1$°C/min). **Figure 3** shows the polarizing optical microscope images of D2-6PC5 under crossed polarizers during slow cooling from the isotropic melt. The focal conic texture disappeared and the area of a dark field gradually expanded. The typical cross isogyre was observed in the dark field by conoscopic observation under a polarizing optical microscope. From these results, we confirmed the homeotropic orientation of D2-6PC5 between bare glass surfaces.

These orientation behaviors are strongly influenced by the mesogenic phase structure. **Table 1** also lists the tendency to exhibit spontaneous homeotropic orientation together with the phase sequences. Among the D2-6X series, homeotropic orientation was observed for X = PPCN, PC5, and Azo5 as well as D2-10PPF$_2$O4. These dendrimers exhibited relatively wide temperature ranges of the SmA phase. On the other hand, the mesogens, PPO1 and PPF, showed a narrow SmA temperature range and no SmA phase, respectively. The similar tendency was more clearly observed in D2-*n*PC5 series. D2-12PC5, whose SmA range is only 7–8 K, did not

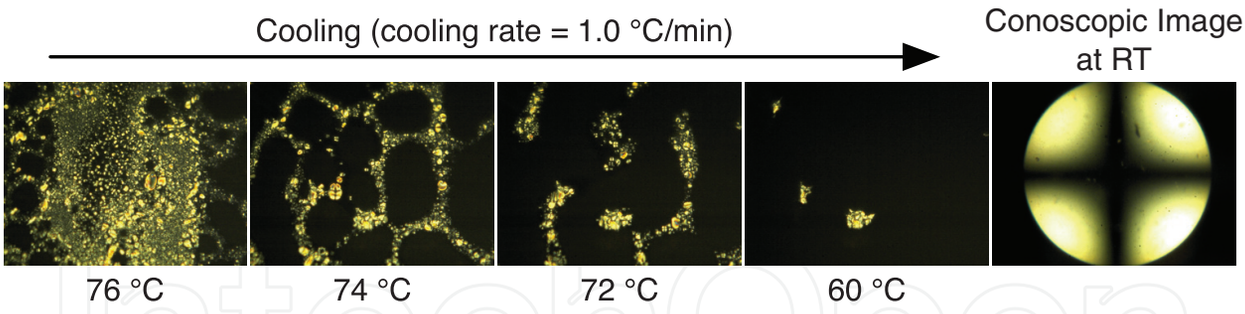

Figure 3. Photomicrographs of D2-6PC5 under crossed polarizers during slow cooling from the isotropic melt (from left to right, DT = −1°C/min). A conoscopic image at room temperature is also shown on the right.

exhibit the homeotropic orientation. In contrast, D2-*n*PC5's with $n = 3$ or 6 have a wide SmA range of around 50 K, and show good spontaneous homeotropic orientation. Therefore, the spontaneous homeotropic orientation seems to be realized in mesogens with the stable SmA phase, in which mesogens can easily move within the SmA layer structure rather than in the more highly ordered SmB or SmE phases. However, D2-6BPO1 did not show homeotropic orientation, although it exhibited the stable SmA phase. Thus, the orientation might require the alkyl termini longer than four carbons like PC5, Azo5, and PPF_2O4. The effect of the generation can be seen in D*G*-10PPF_2O4 ($G = 1$–5): the 1st and the 5th generation dendrimers did not align homeotropically. The former ($G = 1$) may not form well-ordered smectic structure. As for the latter ($G = 5$), the molecule is so large that the molecule becomes a spherical shape due to the steric repulsion between the terminal mesogens.

3. Application for liquid crystal alignment

The present dendrimers have an advantage for providing spontaneous LC alignment at surfaces and interfaces. In other words, no pretreatment of surfaces is necessary for obtaining good alignment. This advantage can be used for manufacturing LC displays. In this section, we introduce two applications of dendrimer molecules for LC alignment; LC displays and controlling physical parameters of LC cells.

The first issue to be discussed is how dendrimer molecules align at surfaces. Based on X-ray diffraction measurements, Li et al. [15] assigned a strong diffraction peak in a small angle region to $n = 2$ and concluded the periodicity corresponds to a stretched structure shown in **Figure 4(a)** [15]. However, other researchers assign this peak to $n = 1$ [16] and the periodicity is concluded to a half the stretched molecular length. Hence, the surface structure could be **Figure 4(b)** [17] or **Figure 4(c)** [18]. Additional important information for the surface structure is that the surface with azodendrimers is optical second-harmonic generation (SHG) active. **Figure 5** shows SHG intensity as a function of UV intensity [19]. The film is SHG active without UV irradiation. This is consistent with the models shown in **Figure 4(b)** and **(c)**. With increasing UV light intensity, SHG activity decreased. This is because the transformation to the *cis*-form destroys the polar orientation order. Further details are a future problem.

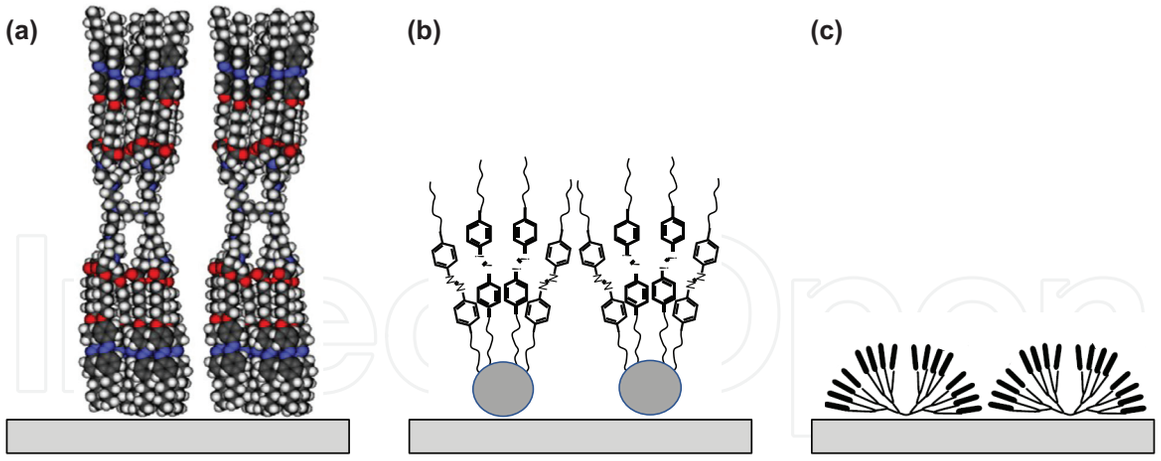

Figure 4. Model structures of dendrimer molecules adsorbed on a surface, (a) symmetric shape [15], (b) asymmetric shape [17], and (c) asymmetric fan shape [18]. Copyright 2012, American Chemical Society [15], Copyright 2015, National Academy of science [17], and Copyright 2014, Optical Society of America [18].

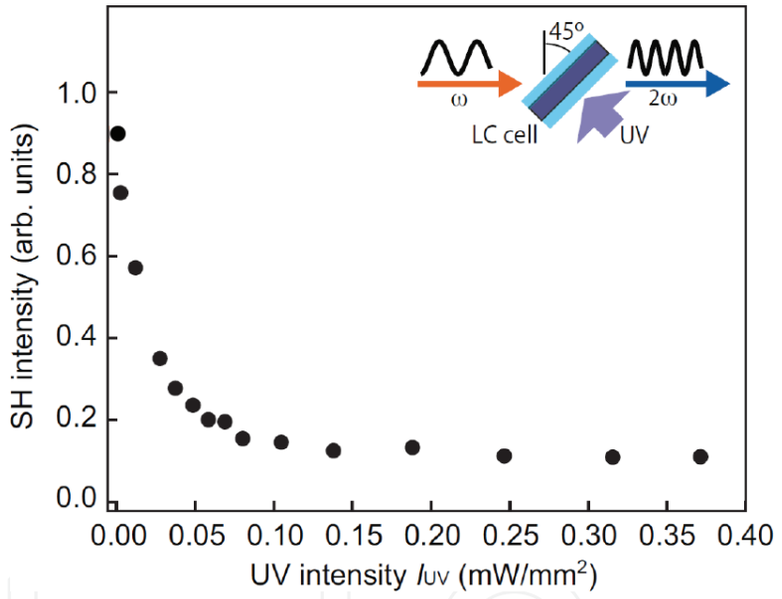

Figure 5. SHG intensity as a function of UV intensity [19]. Optical geometry is also shown in the figure. Copyright 2017, Royal Society of Chemistry.

3.1. Application for liquid crystal display

LC displays are essentially driven by an electric field. Hence, photo-induced switching is not relevant in LC displays. However, to introduce the capability of spontaneous alignment of LCs at surfaces/interfaces by the present dendrimers, we cannot avoid the description of the LC display application using dendrimers with and without azo linkages (see **Figure 2**).

The most important property is spontaneous adsorption of dendrimers onto substrate surfaces, resulting in spontaneous homeotropic alignment of LCs, which makes pre-surface treatment-free or polyimide-free LC displays possible [20]. The process of LC introduction into

an empty cell shown in **Figure 6(a)** and **(b)** are illustrations of the initial and final stages of the introduction of LCs containing dendrimers, respectively [21]. A corresponding texture is shown in **Figure 6(c)** [22]. In the injected area (right), homeotropic alignment is realized, but in the area far from the entrance (left), planar alignment is obtained because of the lack of surface coverage by dendrimers.

The application of dendrimers to a LC display was first reported in IDW (International Display Workshop) in 2011 [20]. Since the unperturbed state is homeotropic, application is principally possible for vertical alignment (VA) mode. The main advantage is of course polyimide-free spontaneous homeotropic (vertical) alignment just by dissolving dendrimers in LCs used. Momoi et al. [20, 21, 23] used a large glass substrate with dimensions 100 mm × 100 mm and large ITO interdigitated electrodes used for the in-plane switching (IPS) mode. The electrode with the gap of 10 μm covers a 10 mm × 10 mm area. **Figure 7** shows photographs of (a) off and (b) on states of a test cell of an LC mixture ZLI-4792 (Merck) containing 1% D2-6PC5 (see **Figure 2**) [20, 23]. The corresponding orientation change during the electro-optic switching between dark and bright is illustrated in **Figure 7(c)** and **(d)** [24]. A polarizing microscope image and a temporal electro-optic response behavior are shown in **Figure 8** [18].

An important question for practical applications is whether this method using dendrimers is applicable for all LCs and surfaces or not. Haba et al. [18] addressed this question. They used two dendrimers (D2-6PPCN and D2-6PC5) as shown in **Figure 2**, and two LCs; 4′-cyano-4-n-penthylbiphenyl (5CB) and a mixture ZLI-4792. Although 5CB could dissolve both dendrimers,

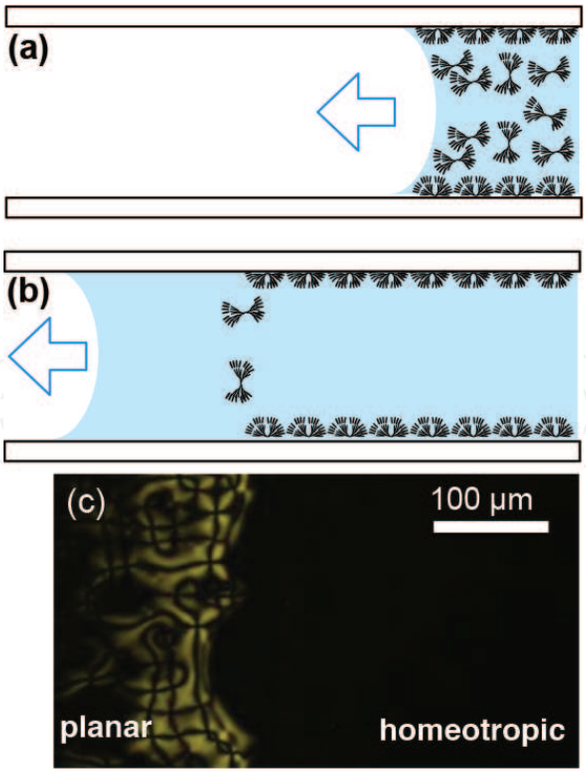

Figure 6. Cartoons showing the introduction of LC with dendrimers into a cell; (a) initial and (b) final stages. Actual photomicrograph image corresponding to (b) is also shown in (c).

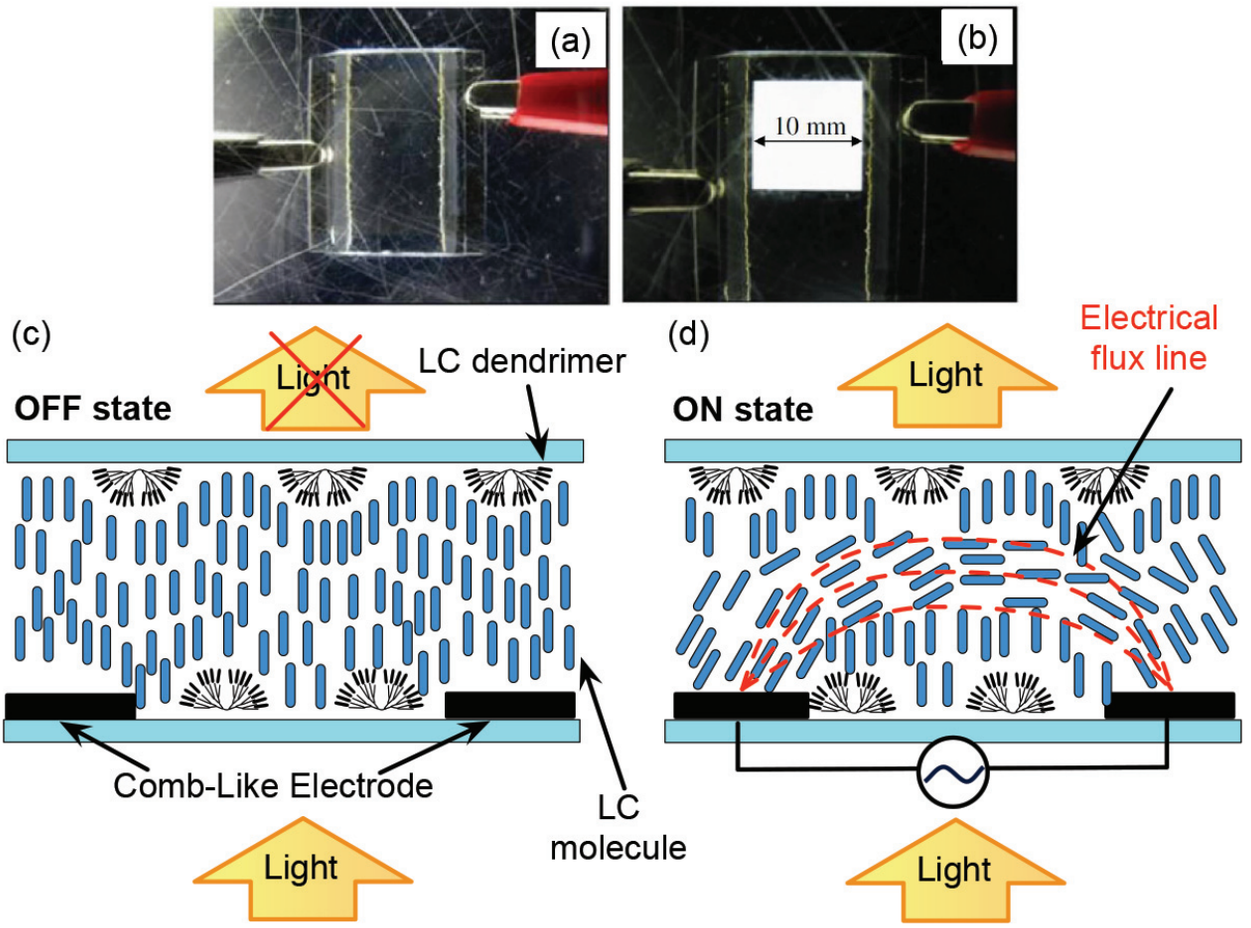

Figure 7. Electro-optic performance. Photographs of (a) off and (b) on states of a test cell [23]. The corresponding sectional images of the director orientations are also shown in (c) and (d), respectively. Copyright 2012, Society for Information Display.

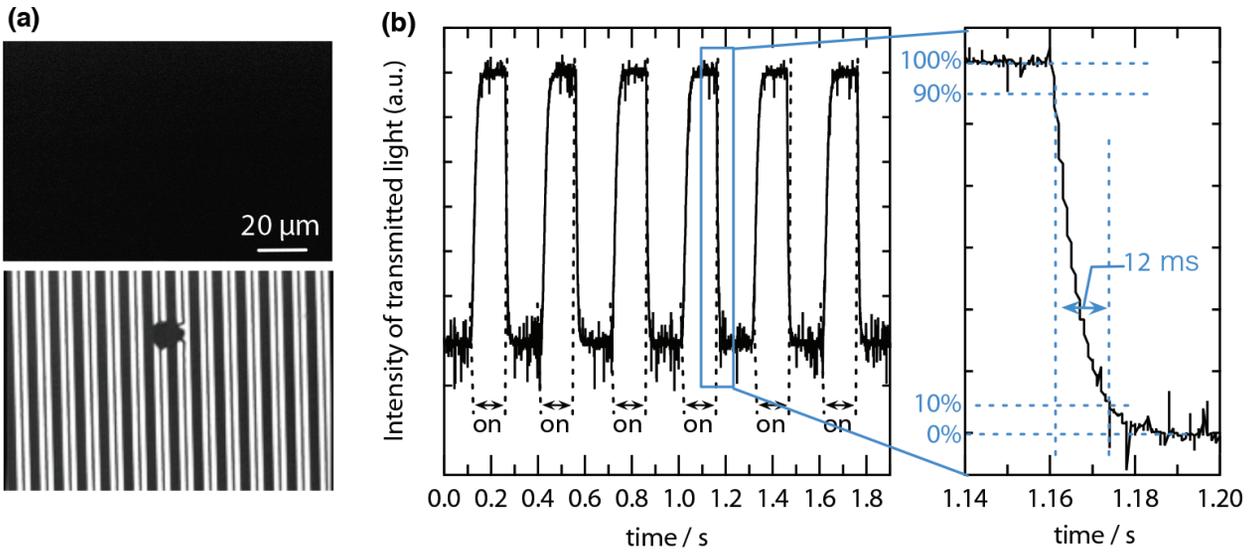

Figure 8. Electro-optic response [18]. (a) Polarizing optical microscope images in off (upper) and on (lower) states. (b) Temporal transmittance changes during sequential electric field application and termination. Copyright 2014, Optical Society of America.

D2-6PCN was not soluble in ZLI-4792. Both D2-6PPCN/5CB and D2-6PC5/ZLI-4792 gave good homeotropic alignment in the absence of an electric field. The surface free energy of substrates was found to be another important factor for good homeotropic alignment. Examination of contact angles for various surfaces showed that hydrophilic surfaces are important for good homeotropic alignment.

Another question is a possible use of azodendrimers for planar alignment, which is necessary for the twisted nematic (TN) and IPS modes. A new dendrimer was successfully developed for this purpose [25]. It is well known as a command surface [2] that surface azobenzene layer commands the orientation change from homeotropic-to-planar by photo-isomerization of the azobenzene. A cartoon of this phenomenon in the present azodendrimer case is illustrated in **Figure 9**. For the present purpose of IPS mode displays, however, there are two problems such as (1) prohibiting the relaxation to the *trans*-state and (2) realization of uniform planar orientation.

In order to prevent the relaxation and fix the planar orientation, we introduced a cinnamate group (**Figure 10(a)**), which is expected to dimerize and prevent the transformation of the *cis*-form to the *trans*-form. To examine the LC orientations upon photo-isomerization and relaxation, nematic LC mixture JC-5066XX (JNC, Japan) was doped with 1 wt% azodendrimer (D2-6AzoCin2). Solubility was poor and planar orientation was observed in most of the mixtures. Some of however, showed a good homeotropic orientation as shown in **Figure 10(b)**. Upon UV irradiation, the schlieren texture showing a planar orientation emerged, as shown in **Figure 10(c)**. More importantly, the planar texture remained after 72 days, as shown in **Figure 10(d)**. When we used D2-6Azo5 without a cinnamate group (**Figure 2**), however, stable planar orientation was not obtained after terminating UV irradiation. Thus, the cinnamate group in D2-6AzoCin2 is important for a stable and sustainable planar orientation [25]. We confirmed prolonged stability after 133 days using a different LC mixture (ZLI4792) [25].

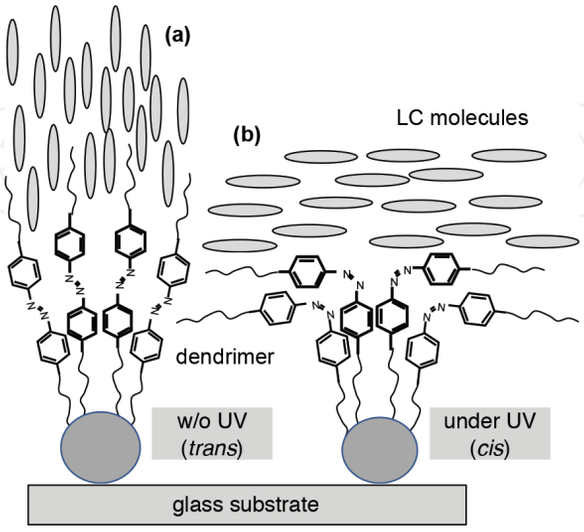

Figure 9. Cartoons showing a command surface effect. (a) Without UV light irradiation, dendrimers are in the *trans*-state, resulting in homeotropic orientation. (b) Unver UV light irradiation, dendrimers are in the *cis* state, resulting in planar orientation.

The second problem, uniform planar alignment, could be solved by using linearly polarized UV light irradiation [25]. Preferential orientation of LCs along the direction perpendicular to the polarization of UV light is well known [3]. The result is shown as photo-micrograph images under crossed polarizers subjected to a rotation of a microscope stage, as shown in **Figure 11**. At angles 0° (parallel to the linear polarization of UV light), complete dark views were obtained. At 45°, bright views due to the birefringence were obtained. Thus, a uniform planar alignment was successfully obtained. Electro-optic response was confirmed to occur. The detailed examination of the electro-optic response is a future problem.

3.2. Application for controlling physical parameters

As mentioned in Section 3.1, the present dendrimer molecules are useful for aligning LCs without pretreatment of surfaces. Initially, the surfaces force LCs to align homeotropically, as mentioned in Section 3.1. If we use azodendrimers, the surface acts as a command surface; UV and VIS light irradiation commands LC molecules to make planar and homeotropic orientations, respectively, due to *trans-cis* photo-isomerization (**Figure 9**). Since LCs have anisotropy,

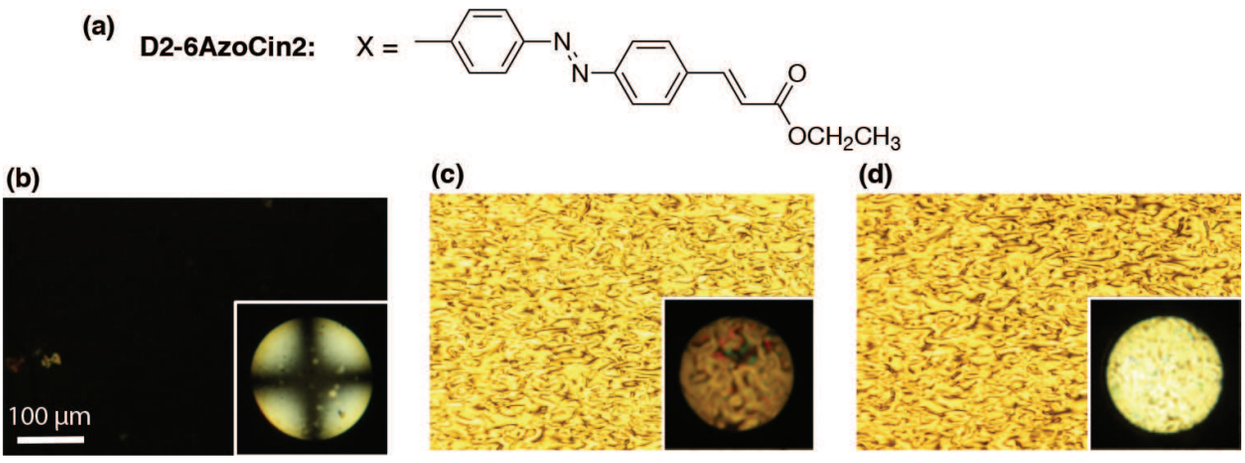

Figure 10. (a) Chemical structure of an azodendrimer with cinnamate tails. Please refer to **Figure 2** for X. Polarizing photomicrographs in (b) without UV light irradiation, (c) immediately after UV light irradiation, and (d) 72 days after terminating UV light. Photos taken by Mr. Shun Sato.

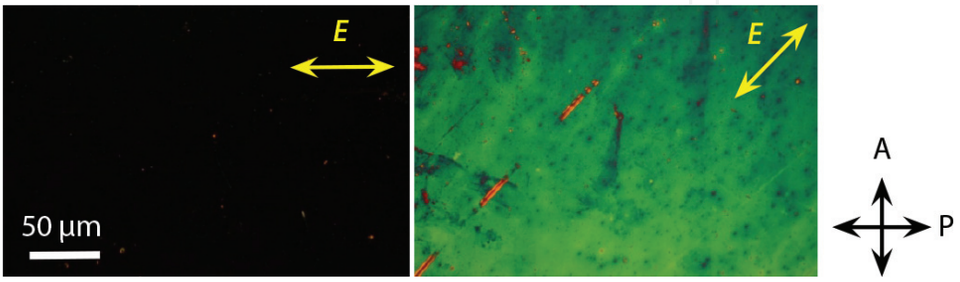

Figure 11. Polarizing photomicrographs of a cell after linearly polarized UV light irradiation. Two images are taken during the cell rotation under crossed polarizers. Photos taken by Mr. Shun Sato.

their physical parameters are also anisotropic. Namely, refractive index, dielectric constant, electric conductivity, etc. have different values depending on the direction with respect to the director. Actually, LC displays utilize the light transmittance change due to refractive index change caused by electric field-induced orientation change. We may find other applications by controlling the physical parameters using external stimuli. An electric field is one of important external stimuli, but is not always necessary. Instead, light irradiation is another useful external stimulus. Here we introduce a possible device using photo-controllable thermal diffusivity [26].

The sample used was 4′-n-pentyloxybiphenyl-4-carbonitrile (5OCB) containing a small amount (0.02 wt%) of azodendrimers. The thermal diffusivity was measured by a temperature wave method [27]. **Figure 12(a)** shows a temperature dependence of thermal diffusivity for a sample under UV (365 nm) light irradiation (cross), under VIS (420 nm) light irradiation (open circle), and without light irradiation (filled circle). It is natural to have a good agreement between the latter two data because of the same homeotropic alignment in both conditions. Photo-induced switching of the thermal diffusivity at 54°C is shown in **Figure 12(b)**. Upon UV and VIS light irradiation, the thermal diffusivity drastically changes almost by two times. The switching speed depends on light intensity. It was found that the switching rate linearly depends on UV and VIS light intensities. Under a moderate light intensity such as 5–10 mW/cm^2, the response time of a few tens of seconds was obtained.

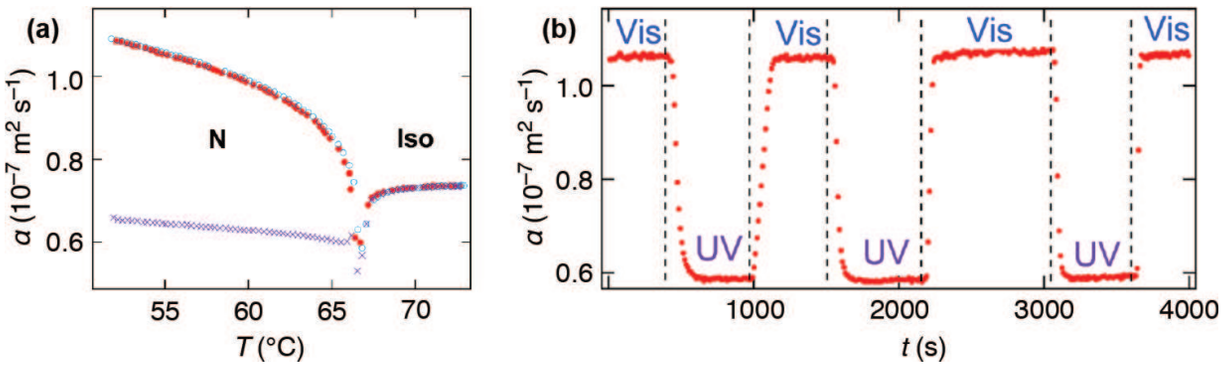

Figure 12. (a) Temperature dependence of thermal diffusivity under UV light irradiation (cross), under VIS light irradiation (open circle), and without light irradiation (filled circle). (b) Photo-induced temporal change of thermal diffusivity [26]. Copyright 2015, AIP Publishing.

4. Photo-triggered surface dewetting

One of the important applications of azo molecules is a surface relief grating formation, which is based on the phenomenon of photo-induced mass migration in azo-containing polymer films [28], low-molecular-mass azo compounds [29], and even in dendron-containing compounds [30]. According to Seki et al. [31], the mass migration in liquid crystalline azo-polymers is highly sensitive to UV light compared with conventional amorphous polymer films. In this sense, the azodendrimer systems are a very attractive candidate for efficient mass migration upon UV light irradiation.

For experiments [15], quartz substrates were properly cleaned to be hydrophilic. Chloroform solution of azodendrimers was spin coated on such substrates. The samples were subjected to UV light irradiation.

Figure 13 shows atomic force microscopy (AFM) images of D2-6Azo5 after UV light irradiation under different conditions. The morphological change is remarkable, exhibiting the surface dewetting and providing a number of separated domains of a few micrometers [15]. Note that a linear polymer of almost identical molecular mass showed no change under the same experimental condition. Another important condition is the hydrophobicity of the substrate. No dewetting behavior was observed under the same experimental condition when hydrophobic surfaces were used. The morphological structure depends on many factors such as UV intensity, irradiation duration, film thickness, etc. The initial flat surface started to change above UV light intensity of 150 mJ cm^{-2}. First, holes grew, coalesced, and formed dome structures with increasing UV light intensity. Under UV light intensity of 400 mJ cm^{-2}, the dome height reached 770 nm, which was about eight times of the initial film thickness. The film thickness dependence of the morphology is shown in **Figure 13(a)**. With increasing the film thickness, the dome size increased and the dome density decreased. The films thicker than 100 nm did not show dewetting. Instead, some protrusions of several micrometers diameters were observed on the film surface. Patterned structure formation such as a surface relief grating is also possible using patterned UV light irradiation through photomasks. The result reflects the film thickness dependence. Namely, as shown in **Figure 13(b)**, hierarchical morphologies were observed in films thinner than 100 nm, but ordinary surface relief grating was formed in a film of 120 nm thick.

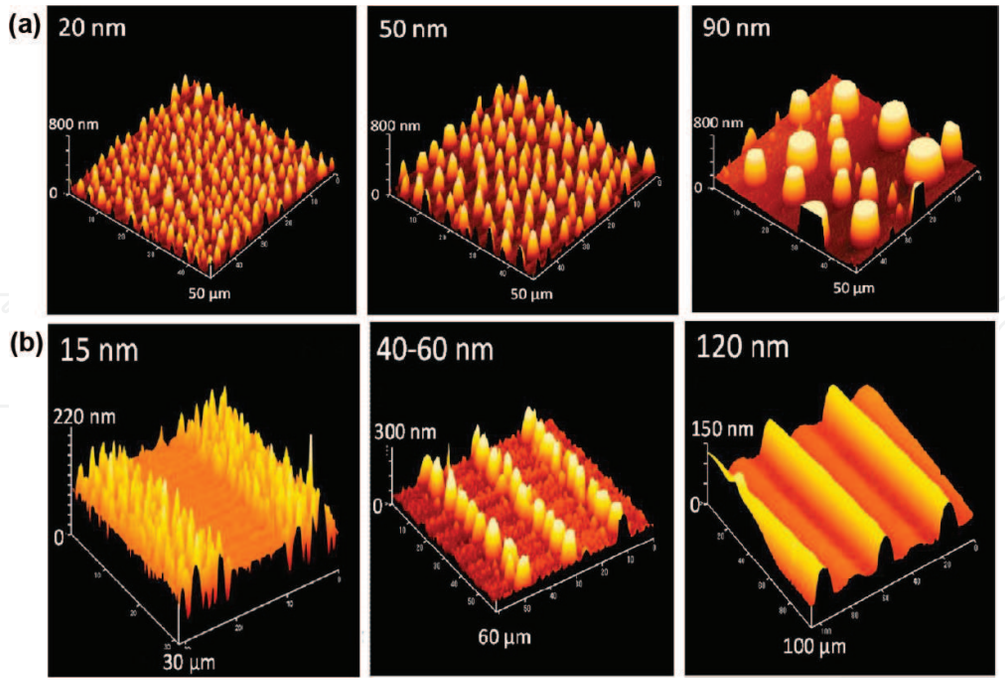

Figure 13. AFM images of azodendrimer surface layer with different thicknesses after UV light irradiation [15]. (a) Uniform and (b) patterned UV light irradiation. A sample with a 120 nm thick layer in (b) shows a simple conventional surface relief grating. Copyright 2012, American Chemical Society.

5. Memory device

LC devices are usually fabricated as sandwich cells with different surface orientations planar, homeotropic, and hybrid orientations obtained using two planar surfaces, two homeotropic surfaces, and (planar/homeotropic) surfaces, respectively. If we can manipulate the surface orientation locally, we can make memory devices. LC displays are one of the examples, where an electric field is applied using matrix-type electrodes to change the LC orientation locally. In this case, however, the perturbed LC orientation returns back to the original one after terminating the field, since the stable orientation is guaranteed by the surface anchoring condition. Using light irradiation is another useful technique for driving devices.

We proposed a novel bistable device using an anchoring transition and a command surface [32]. This device (**Figure 14(c)**) has advantages compared with devices, which use only anchoring transition (**Figure 14(a)**) [33] or command surface (**Figure 14(b)**) [2]. Here the anchoring

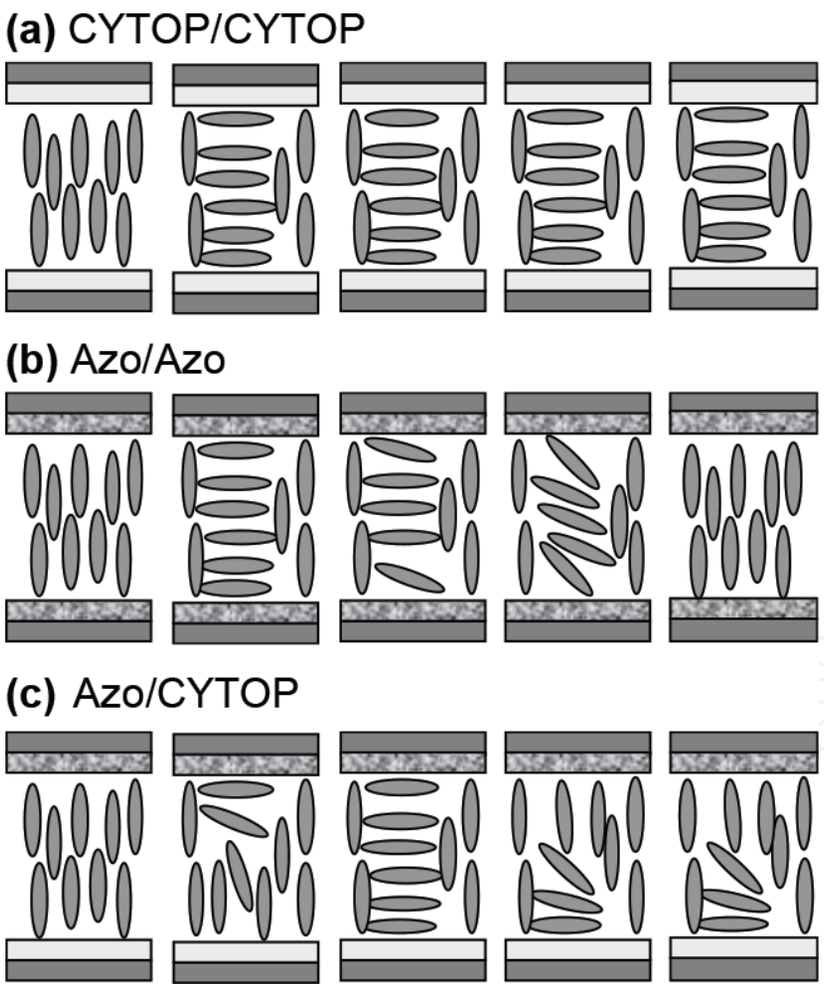

Figure 14. Cartoons showing orientation change upon UV light irradiation and termination (from left to right) in three cells with different surface layers; (a) CYTOP/CYTOP, (b) azodendrimer/azodendrimer, and (c) azodendrimer/CYTOP hybrid. Intense light irradiation is needed for an orientation change in (a). An induced planar orientation relaxes back to a homeotropic orientation in (b). A hybrid orientation is established and preserved in (c).

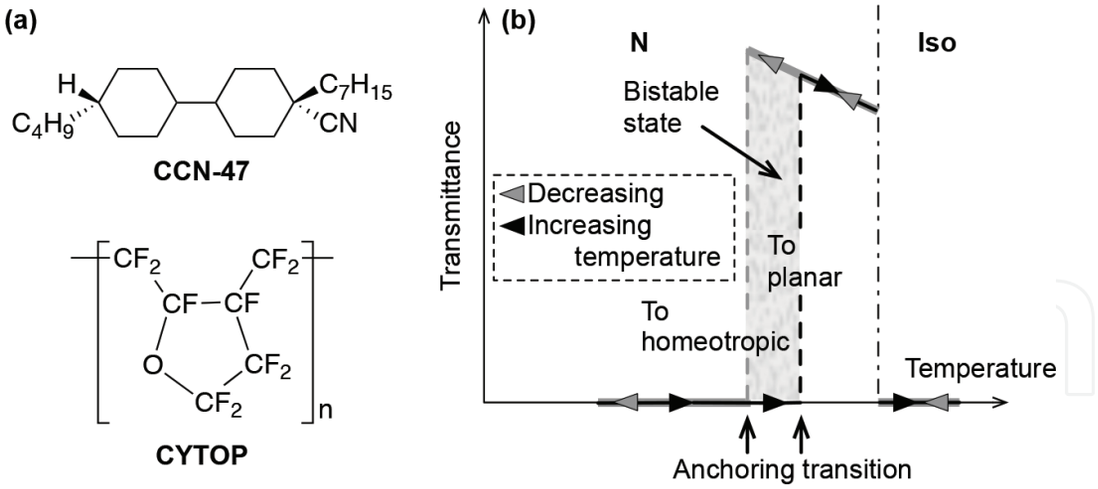

Figure 15. (a) Molecular structures of a LC compound (CCN-47) and a surface layer (CYTOP). The LC cell with the combination of CCN-47 and CYTOP exhibits a discontinuous anchoring transition. (b) Cartoon illustrating a discontinuous anchoring transition with a bistable temperature range (hatched area).

transition we used was a spontaneous discontinuous orientation transition between planar and homeotropic orientations. This phenomenon was clearly observed in a commercial compound 4′-butyl-4-heptyl-bicyclohexyl-4-carbonitrile (CCN-47, Merck) sandwiched by glass substrates with poly[perfluoro(4-vinyloxy-1-butene)] (CYTOP, Asahi Glass) (**Figure 15(a)**) on their surfaces [33]. As schematically shown in **Figure 15(b)**, the transmittance of the cell between crossed polarizers appears at the Isotropic (Iso)-nematic (N) transition, and suddenly drops to zero by decreasing temperature. This process is the manifestation of a discontinuous anchoring transition from planar to homeotropic alignment. On heating, the reverse change is observed at different temperatures. This means that there exists a temperature range (hatched area in **Figure 15(b)**) showing bistable states, where both planar and homeotropic orientations are stable. The existence of the bistable states provides us with a bistable memory device [34].

We constructed a hybrid cell consisting of CYTOP-coated and bare glass substrates (**Figure 14(c)**) and introduced a small amount (0.05 wt%) of azodendrimer molecules into the CCN-47 host [32]. In this cell, we confirmed stable performance as a memory device, as described in the following. First, the hybrid cell was cooled to room temperature. At this condition, the homeotropic orientation was realized. Then the cell was heated to a bistable temperature region, keeping the homeotropic orientation (dark view under crossed polarizers). UV light irradiation onto the cell induced the anchoring transition at the azodendrimer surface. The orientation change to a planar state propagated to the opposing surface, resulting in a bright spot. Since the anchoring transition is light-driven, the UV light intensity was very low (35 μW/mm^2), compared with laser (heat)-driven anchoring transitions (1 kW/mm^2) [34]. Hence, the present hybrid device is advantageous to the devices using only the anchoring transition (**Figure 14(a)**).

The advantage of the hybrid device over the device using only command surfaces (**Figure 14(b)**) is clear. If we use sandwich cells with azodendrimer-attached surfaces in both sides without using CYTOP, the azodendrimers play as a command surface, that is, a homeotropic-to-planar

orientation change occurs locally at the spot under UV irradiation. However, the life time of the *cis* (excited) state is finite, a few minutes to an hour depending on LCs (solvents) used. Hence, the planar orientation relaxes to the homeotropic orientation with time. On the contrary, the planar orientation at the CYTOP surface is very stable in the bistable temperature range. Hence after the relaxation to the *trans*-state at the dendrimer surface, a hybrid orientation, namely a homeotropic orientation at the dendrimer surface and a planar orientation at the CYTOP surface, is stabilized. The advantages of the present hybrid cell over cells with only CYTOP surfaces or only azodendrimer surfaces are clearly displayed in **Figure 14**. In this way, azodendrimer surfaces provide us with highly photo-sensitive surface for writing in devices keeping the memory capability using the anchoring transition phenomenon.

6. Photo-switching of liquid crystal orientation in different geometries

The azodendrimer command surface facing to LCs makes photo-switching of LC orientation possible, as mentioned above (see **Figure 9**). This phenomenon is well known on flat substrate surfaces, which are necessary to be coated with azo molecules before fabricating cells [2]. The present azodendrimers have a characteristic feature that the azodendrimer molecules are spontaneously adsorbed at interfaces. This means that we need no pretreatment of surfaces. Moreover, the molecules can be attached at interfaces, which we cannot intentionally treat beforehand, such as liquid/liquid interfaces. Only thing we have to do is just dissolving the azodendrimer molecules into LCs before preparing samples. Four examples are introduced in the following.

6.1. Defects in liquid crystal droplets

If LC molecules are mixed with other liquid materials such as water or glycerol and stirred, LC forms droplets with different sizes (**Figure 16(a)**). The formation of LC microdroplets with a

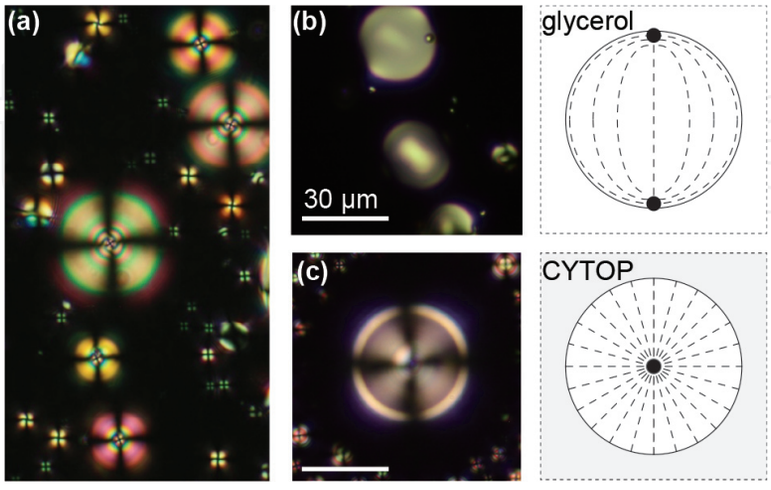

Figure 16. (a) Photomicrograph of LC droplets in water. Photomicrographs of a droplet of 5CB in (b) glycerol and (c) CYTOP [22]. If 5CB is doped with azodendrimers and is dispersed in glycerol, a radial orientation is realized like in (c). The structure changes from radial-to-bipolar by UV irradiation like in (b) [22]. Copyright 2013, John Wiley & Sons, Inc.

uniform size is one of topical fields, that is, microfluidics, which are interesting both from basic science and various applications [35].

The studies of LC microdroplets have been conducted since long time ago [36]. The LC orientations at interfaces are fixed when background liquid is chosen: LC molecules orient tangentially at glycerol interfaces. On the other hand, in aqueous solutions and hydrophobic polymer CYTOP, LC molecules align normal to the interface. Under crossed polarizers, LC droplets in glycerol and CYTOP show a bipolar image and a dark cross, respectively, being characteristic of tangential and radial molecular orientations, respectively, as shown in **Figure 16(b)** and **(c)** [22]. In previous studies, fixed surface conditions were used except for a work by Yamamoto et al. [37]. We introduced the azodendrimer molecules into host LCs, which provide normal orientation of LCs at droplet surfaces. In addition, planar orientation is induced by irradiating the droplet with ultraviolet (UV) light. We showed the orientation change of LCs upon UV and visible (VIS) light irradiation in three phases, nematic (N), cholesteric (Ch), and smectic A (SmA) [22], which will be described in the following. We used 5CB for the N phase. For a cholesteric material, a chiral dopant CB15 (Merck) was added to 5CB. For smectic A (SmS) materials, 4′-n-octyl-4-cyanobiphenyl (8CB) was also used. The dendrimer molecules added in LC hosts were 0.1–0.3 wt% of D2-6Azo5.

In the N phase, the textures are similar to **Figure 16(b)** and **(c)** under UV and VIS (or before UV irradiation), respectively [22]. In the Ch phase, concentric rings were observed when the sample was irradiated with UV light (**Figure 17(a)**), although they are vague because of a short helical pitch. If we use a Ch LC with a longer pitch, clear concentric rings with a periodic space are observed, as shown in **Figure 17(c)**. Under UV light, the surface orientation is planar (see

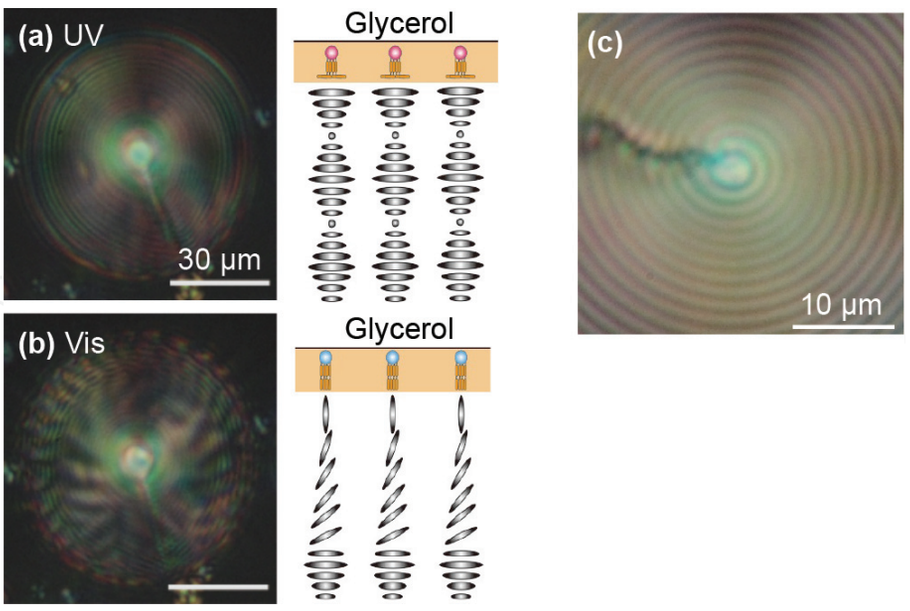

Figure 17. Photomicrographs of a droplet of a cholesteric LC-containing azodendrimers under (a) UV and (b) VIS light irradiation [22]. Schematic illustrations of molecular orientations corresponding to (a) and (b) are also shown on the right [22]. (c) Photomicrograph of a droplet of a cholesteric LC with a long helical pitch containing azodendrimers [22]. Concentric rings showing a helical structure with a helical axis along the radial direction are clearly seen. Copyright 2013, John Wiley & Sons, Inc.

Figure 17(a) right), so a helical structure with the helical axis along the radial direction is formed. Since the planar surface orientation overall the droplet surface inevitably induces defect(s), at least one defect line from the center of the droplet toward the surface emerges, as clearly seen in **Figure 17(c)**. The situation is more complicated under VIS light. The helical structure remains at least in the central region, which is identified by remaining concentric rings. The helical structure is disturbed from the surface region, where homeotropic orientation is achieved (see **Figure 17(b)** right). Many dark lines showing defects are observed in the texture (see **Figure 17(b)** left) [22].

In the SmA phase, the deformation is serious under UV light. Since the surface orientation is homeotropic under VIS light, an onion-like smectic layer structure is formed with the director being parallel to the radial direction (**Figure 18(b)**). A large extinction cross is a manifestation of the concentric SmA layer structure. Here the splay deformation of the director within each layer is allowed. The molecular orientation under UV light is complex, because the layer must be perpendicular to the surface. Since the reorientation occurs from the surface, curved smectic layers are formed in the outer region of the droplets, and are connected to concentric layer structure inside the droplets. As shown in **Figure 18(a)** right, many defect lines are formed along the radial direction, and are observed as a microscope image (**Figure 18(a)** left).

Droplet formations of LCs in other phases are interesting topics. Bent-shaped molecules exhibit various phases [38]. Particularly, many phases, in which reflection symmetry breaking occurs, such as the B2, B4, B7, DC (dark conglomerate), and N_{TB} (twist-bend nematic) phases would be interesting. How does chiral segregation occur in droplets, if it occurs? Bent-shaped molecules are also useful for the study of the blue phase (BP), since they stabilize the BP and expand the temperature range. The N phase of bent-shaped molecules also show peculiar

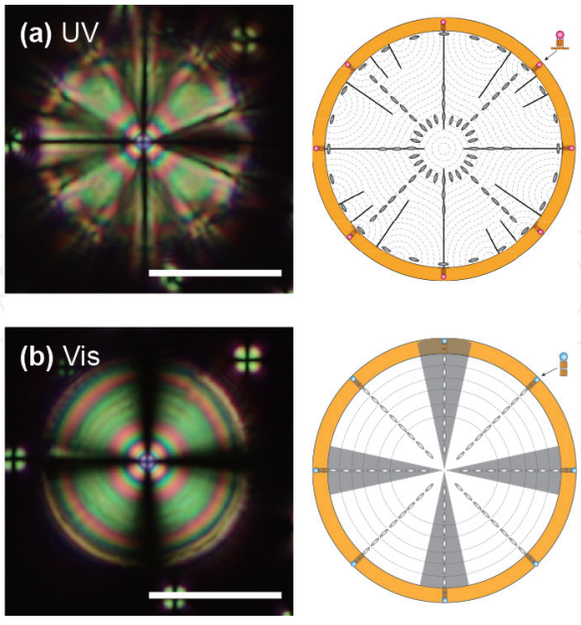

Figure 18. Photomicrographs of a droplet of a SmA LC-containing azodendrimers under (a) UV and (b) VIS light irradiation [22]. Schematic illustrations of molecular orientations corresponding to (a) and (b) are also shown on the right [22]. Copyright 2013, John Wiley & Sons, Inc.

features unlike the conventional N phase. Apart from the bent-shaped mesogens, the relationship between photo-induced reorientation phenomena as a function of elastic constants is another interesting topic. In homeotropic orientation, a splay deformation exists. In contrast, in tangential orientation, a bend deformation is the major component. UV-induced radial-to-bipolar reorientation is strongly suppressed in compounds with huge bend elastic constants compared with splay elastic constants. A compound reported in [39] is an example, in which bend elastic constant is a hundred times larger than splay elastic constants.

6.2. Defects in the vicinity of microspheres

Extensive studies have been made since late 1990s on the defect structures in the vicinity of microspheres [40] and the attractive forces between them [41]. The studies to control the microspheres and the defects around them by external stimuli have been widely made. The external fields used were an electric field [42], laser trapping [43], and thermal gradient [44]. As same as in LC/liquid interface mentioned above, however, the surface of microspheres is normally pretreated to have tangential or homeotropic orientation of LCs. Hence the surface orientation was fixed and no orientation changes have been studied except for the studies by Yamamoto et al. [37]. They observed photo-induced changes of topological defects around colloidal droplets dispersed in azobenzene-containing LCs. In our dendrimer case, photo-controllable interfaces can be provided just by introducing a small amount of azodendrimers into a LC host. The results are shown in [45].

The sample used was 5CB mixed with 0.1 wt% of azodendrimers (D2-6Az05) and a small amount (volume fraction of about 2×10^{-4}) of silica microparticles (about 3 μm in diameter). The sample was introduced into an empty cell of 25 μm thick with rubbing treated planar surfaces. **Figure 19** shows microscope images under crossed polarizers without (a)–(c) and with (d)–(f) a waveplate inserted along the direction diagonal to the crossed polarizers [45]. From the left to right, the temporal changes before ((a) and (d)), during ((b) and (e)), and after ((c) and (f)) UV irradiation are shown. These images are consistent to the defect structures, hedgehog, boojum, and Saturn ring, shown in Figure 19(g)–(i), respectively. Before UV irradiation (g), azodendrimers at surfaces are in a *trans*-state, providing a homeotropic orientation. During UV irradiation (h), *trans*-to-*cis* photo-isomerization leads to a planar (tangential) orientation. Once the azodendrimers at the surface relax to a *trans*-state, a homeotropic surface is realized. Then, the symmetric boojum structure never returns back to the asymmetric hedgehog structure, but to the symmetric Saturn ring structure. Hence, only the transformations between the boojum and the Saturn ring occur by the subsequent UV light on/off.

The response time upon light irradiation is dependent on the UV light intensity and is quite fast under high intensity UV irradiation, as shown in **Figure 20** [45]. The response is nearly exponential (**Figure 20(a)** inset). All processes complete within a one video frame (66 ms). Interestingly, the square of the switching rate is proportional to UV intensity (**Figure 20(b)**).

Let us consider the UV light intensity dependence of the response time assuming a two-level model (**Figure 21**). Here, k_{tc} and k_{ct} are the transition coefficients from *trans*-to-*cis* by UV light and from *cis*-to-*trans* by VIS light, respectively. k_r is a relaxation rate. The rate equation is given by.

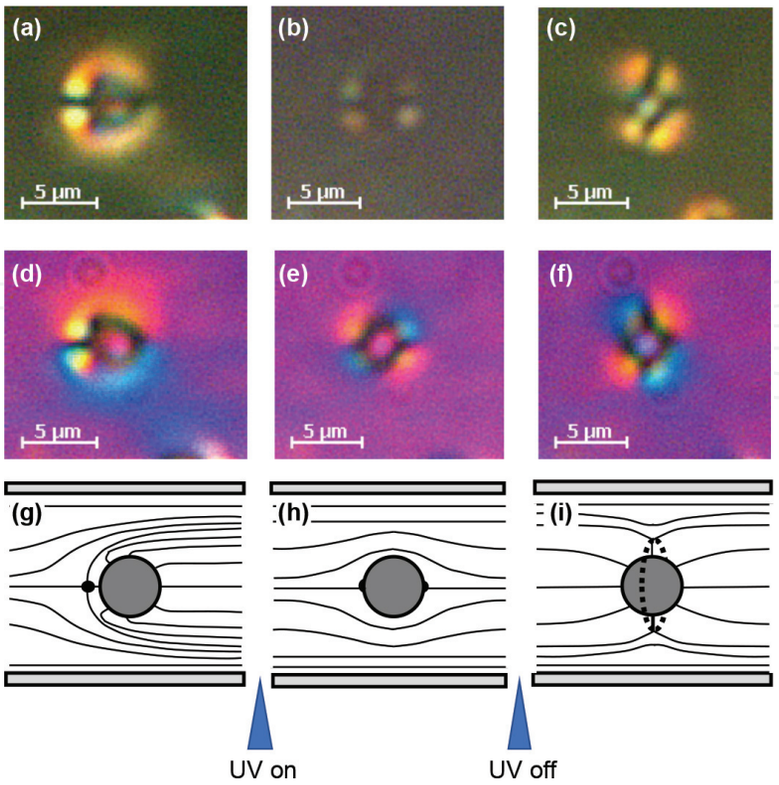

Figure 19. Photomicrographs showing defect structures around a microsphere under crossed polarizers (a)–(c), with a waveplate (d)–(f). A hedgehog defect (g) corresponding to (a) and (d) is observed before UV irradiation. A boojum defect (h) corresponding to (b) and (e) is observed during UV irradiation. A Saturn ring defect (i) corresponding to (c) and (f) is observed after turning off the UV irradiation [45]. Copyright 2014, Optical Society of America.

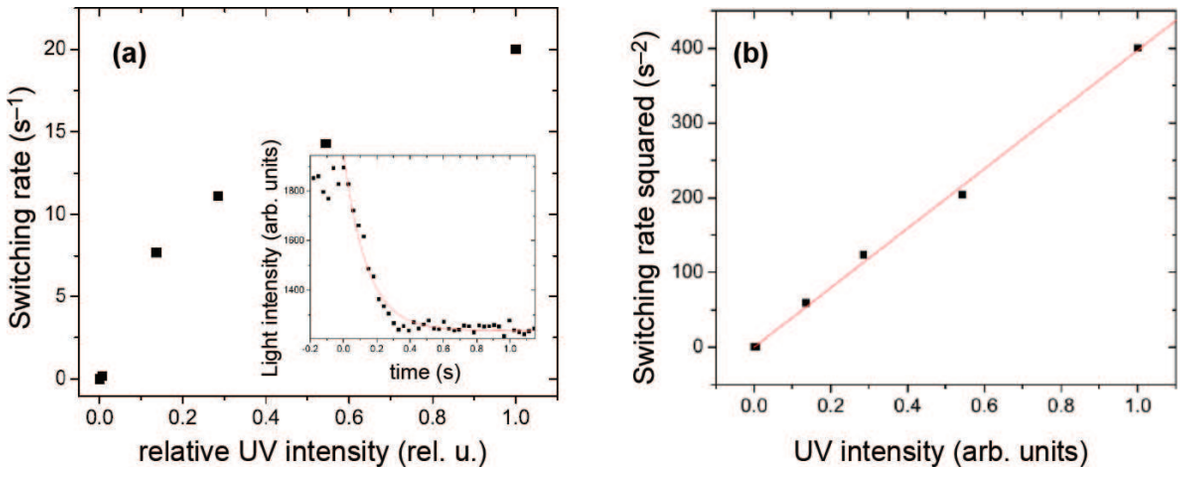

Figure 20. (a) Switching rate as a function of UV light intensity. Temporal change of transmittance is also shown in an inset. (b) Square of the switching rate as a function of UV light intensity [45]. Copyright 2014, Optical Society of America.

$$\dot{n_c} = k_{tc} I_{UV} n_t - k_{ct} I_{VIS} n_c - k_r n_c. \quad (1)$$

Here, n_t and n_c are numbers of *trans* and *cis* molecules, n is a total number of molecules ($n = n_t + n_c$), and $I_{UV/VIS}$ are UV/VIS light intensity. By neglecting the second (no VIS irradiation) and third (very long relaxation time) terms, we obtain.

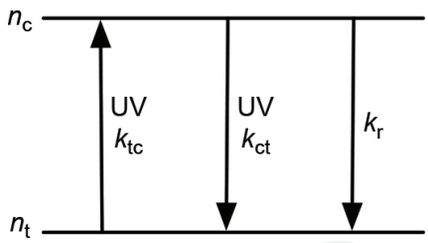

Figure 21. Two-level model for photoisomerization process.

$$n_c = n\left[1 - \exp\left(-\frac{t}{\tau}\right)\right]. \tag{2}$$

The exponential change shown in the inset of **Figure 20(a)** is reasonable. By using Eqs. (1) and (2) with $k_r = 0$, we obtain.

$$\frac{1}{\tau} = k_{tc} n I_{UV}. \tag{3}$$

The switching rate $(1/\tau)$ is proportional to the UV light intensity I_{UV}. Experimentally, however, $(1/\tau)^2$ is proportional to I_{UV}. The discrepancy may be attributed to the assumption $I_{VIS} = 0$ used. Actually, the experiments were made under VIS light from an optical microscope lump, which always induced the *cis*-to-*trans* transition.

6.3. Defects in the vicinity of microrods

The studies of microrods in LCs are much minor [46]. Here we first describe the defect structures around a microrod and their photo-induced changes [17]. Silica microrods used have their length of 10–20 μm and their diameter of 1.5 μm. **Figure 22** shows micrographs of a microrod in a homeotropically aligned LC cell and the director map around the rod. The background under crossed polarizers is dark because of the homeotropic alignment of LCs

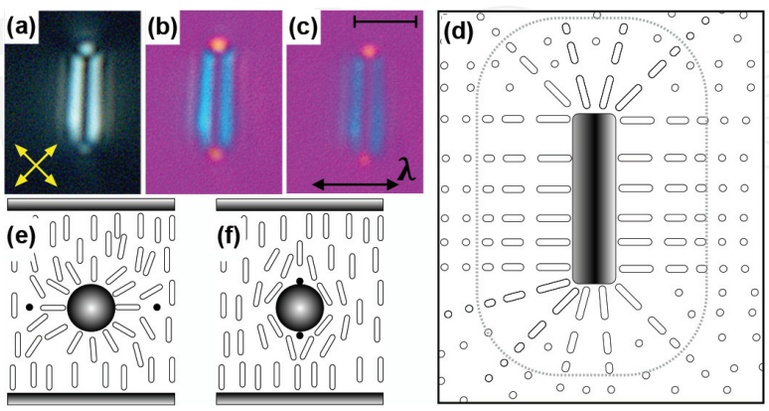

Figure 22. Photomicrographs of a nematic LC with a microrod in a homeotropic cell and corresponding director maps. Micrographs under (a) crossed polarizers, (b) and (c) with a waveplate. Before (a) and (b) and after (c) UV irradiation. Top view of the director orientations before UV irradiation is shown in (d). Side views before and after UV irradiation are shown in (e) and (f), respectively (SI in [17]).

(**Figure 22(a)**). The regions, where LC molecules orient along nearly 45° with respect to the polarizers, are brightest because of birefringence. The insertion of a waveplate gives a blue color at the sides of the rod and an orange color at the edges of the rod, being consistent with the director map shown in **Figure 22(d)**. **Figure 22(e)** is another view of the molecular orientation structure, where two defect lines perpendicular to the image plane (along the rod) are shown as dots.

Upon UV light irradiation, the blue color becomes lighter, but the blue and orange colors themselves do not change. This means that the LC molecules (director) do not orient along the long axis of the rod, but align tangentially perpendicular to the long axis, as shown in **Figure 22(f)**. In this situation, the slow and fast axes of the index ellipsoid do not change but the birefringence becomes smaller, being consistent with the microscope image (**Figure 22(c)**) and the molecular orientation structure (**Figure 22(f)**).

Next, let us describe the results in cells with planar surfaces [17]. Although the free energy does not depend on the orientation of a microrod sitting parallel to the surfaces in homeotropic cells, it does in planar cells, because the elastic energy of LCs and the energy of defects around the rod depend on how the rod orients with respect to the director. **Figure 23** shows the distribution of the rod orientation observed. Two distribution peaks can be seen at 0° and 60°. Full understanding of this distribution is not easy because of the difficulty particularly of the energy estimation of the defect structures.

Figure 24 shows the orientation field of the director around a microrod; (a) and (c) before UV irradiation and (b) and (d) under UV irradiation, where directors are perpendicular and parallel to the rod, respectively. The director orientations are visualized by green and yellow colors in the images seen with a waveplate, which are the same color as observed experimentally (see the actual microscope images at left top in each subfigure). Under UV irradiation (**Figure 24(b)** and **(d)**), the director changes the orientation to be parallel to the rod. In **Figure 24(b)**, where the microrod is almost parallel to the director, the director deformation is localized only at the edge of the rod, so that no color appears, as actually observed experimentally. If the rod

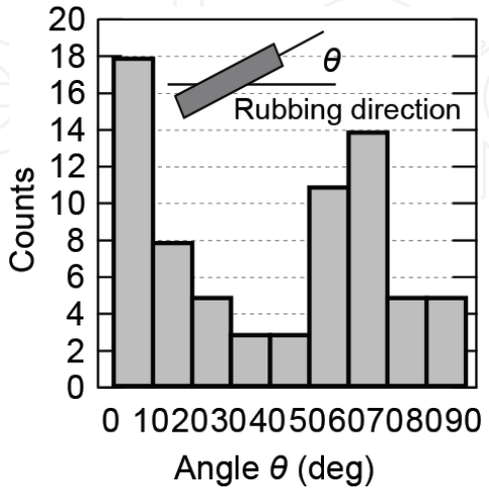

Figure 23. Angular distribution of rod orientation with respect to a rubbing direction (SI in [17]).

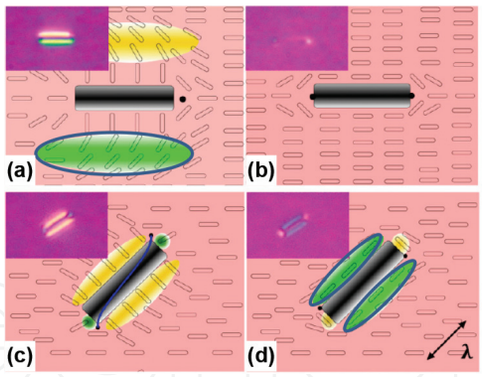

Figure 24. Photomicrographs (left up in each figure) of a nematic LC with a microrod in a planar cell and corresponding director [17]. Copyright 2015, National Academy of Science.

tilts from the director by 45° (**Figure 24(c)** and **(d)**), the director orientation in the vicinity of the rod changes from perpendicular to parallel with respect to the waveplate. Then, a color change from yellow to green occurs, as shown in **Figure 24(b)** and **(d)**. At the edges of the rod, an opposite color change occurs.

Such observations are possible when microrods are somehow fixed at surfaces. When rods are free from surfaces, additional dynamic motions are observed, which are the topics in the next section.

6.4. Dynamic motions of microrods

Figure 25 shows three different dynamic motions of microrods in LCs by UV irradiation [17]. When microrods are parallel to the director, we often observe a lateral motion of the microrods along the director as shown in **Figure 25(a)** and **(b)**. In the other case, the microrod motion appears as its length change (**Figure 25(c)** and **(d)**). This is the result of the rotation of the microrod about its short axis parallel to the surface. The most distinguished motion is

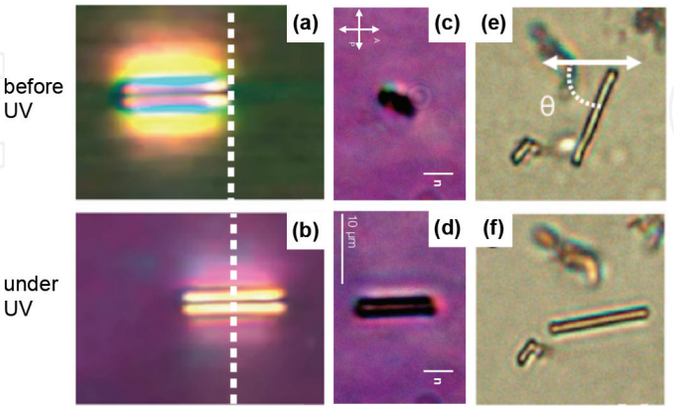

Figure 25. Photomicrographs showing dynamic motions of microrods: (a) and (b) before and during UV light irradiation, respectively, for a lateral motion along the director. (c) and (d) Before and during UV light irradiation, respectively, for a seesaw motion about an axis parallel to a cell surface. (e) and (f) Before and during UV light irradiation, respectively, for a seesaw motion about an axis normal to the cell surface [17]. Copyright 2015, National Academy of science.

http://dx.doi.org/10.5772/intechopen.70715

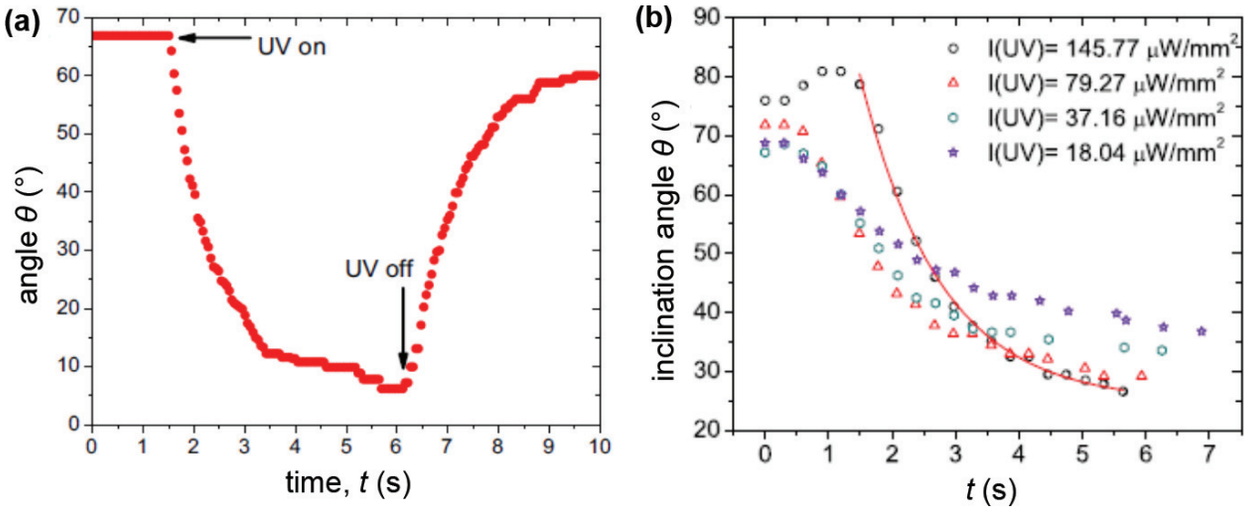

Figure 26. Rotation angle of the seesaw motion of microrods (a) after on and off of the UV light irradiation and (b) the irradiation power dependence [17]. Copyright 2015, National Academy of Science.

observed when rods orient to the direction with finite angles to the director, that is, microrod rotation about its short axis within a plane parallel to the surface (**Figure 25(e)** and **(f)**). The rod returns back to the original direction when UV light is turned off. Thus, the microrods make a seesaw motion by repeated UV light on/off.

The temporal rotation behavior is shown in **Figure 26(a)**, where the angle between the microrod long axis and the director is plotted as a function of time. The rod tends to rotate to the direction parallel to the director (0°) under UV irradiation. When the UV light is terminated, the rod tends to rotate back to the original direction. The rotation speed (response time) is faster and the rotation angle becomes larger with increasing UV light intensity, as shown in **Figure 26(b)**. The solid line in **Figure 26(b)** is the best theoretical fit. The switching angle and the switching rate (inverse switching time) are shown as a function of UV intensity in **Figure 27**. With increasing UV light intensity, the rotation angle becomes larger and the

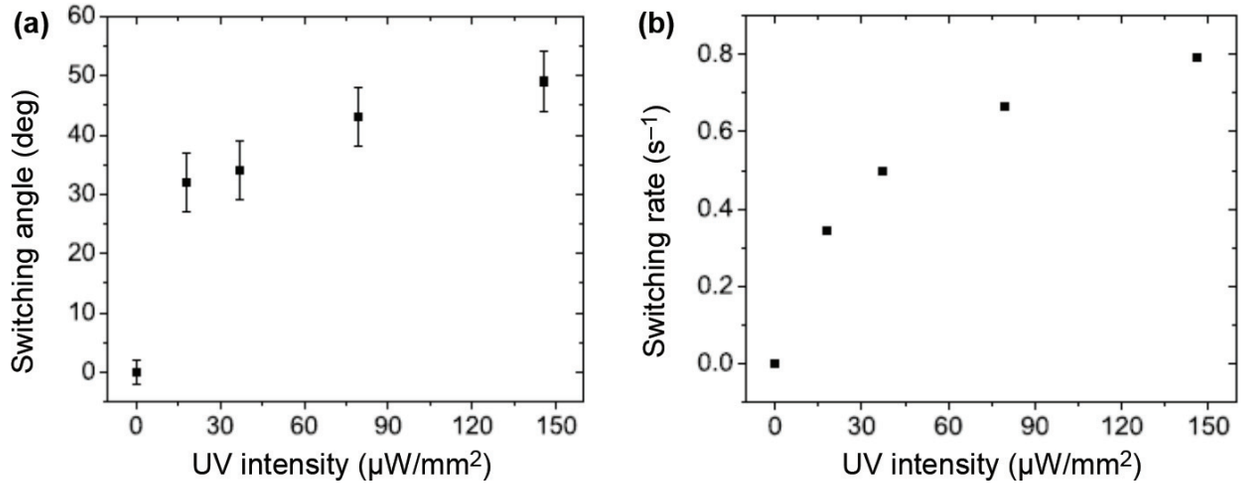

Figure 27. (a) UV intensity dependence of a saturated rotation angle of a microrod. (b) UV intensity dependence of a switching rate of a microrod [17]. Copyright 2015, National Academy of Science.

switching time becomes faster. As will be discussed in Section 7, the anchoring energy $W_a \sin^2\theta$ depends on n_t/n_c; the anchoring strength $W_a = +\infty$ when all azodendrimers are in the *trans*-form, $W_a = -\infty$ when all azodendrimers are in the *cis*-form, and $W_a = 0$ for $n_t = n_c$. At zero I_{UV}, $W_a = +\infty$. With increasing I_{UV}, W_a becomes negative, then the director rotation starts to occur. When the absolute value of W_a is small, the rotational torque is not efficiently transferred to the microrod. Hence the rotation speed is low. With increasing I_{UV}, $| W_a |$ becomes larger and the torque is efficiently transferred to the rod, resulting in faster rotation.

Important difference to the command surface is no use of polarized UV light. In the command surface, linearly polarized UV light irradiation forces the azo linkage to align perpendicular to the polarization direction [3]. On the contrary, linear polarization is not necessary in the present case. However, preferential bending direction in the *cis*-form is automatically chosen by the director field near the surfaces over which azodendrimers cover. Qualitative explanations for the translational and seesaw motions are illustrated in **Figure 28(a)** and **(b)**, respectively. For microrods to make a translational movement, the director field including defect structures must be asymmetric as shown in **Figure 28(a)**. In this case, it is expected that azo groups spontaneously bend (tilt) to a left-hand side upon UV irradiation. This motion forces LC molecules to rotate counterclockwise and clockwise at the upper and lower sides, respectively (1, 2, 3, and 4 in **Figure 28(a)**). The microrod is subjected to an external torque by this rotational motion, resulting in the translational motion to the right.

When the rod is tilted from the director field (**Figure 28(b)**), the director field is oppositely bends at both sides of the rod by UV light, so that the azo groups bend to opposite directions at both sides of the rod, resulting in clockwise rotation of LC molecules. The subsequent torque leads to the rotation of the rod toward the direction parallel to the director. When the UV light is terminated, the rod rotates back to the original orientation shown in **Figure 28(b)**.

Quantitative analysis of the switching behavior was made using a two-dimensional finite element method. With one-constant approximation of elastic constants K, azimuthal angle u of the director field is given by.

$$\Delta u(x,y,t) = \frac{\gamma}{K}\frac{\partial u(x,y,t)}{\partial t}, \tag{4}$$

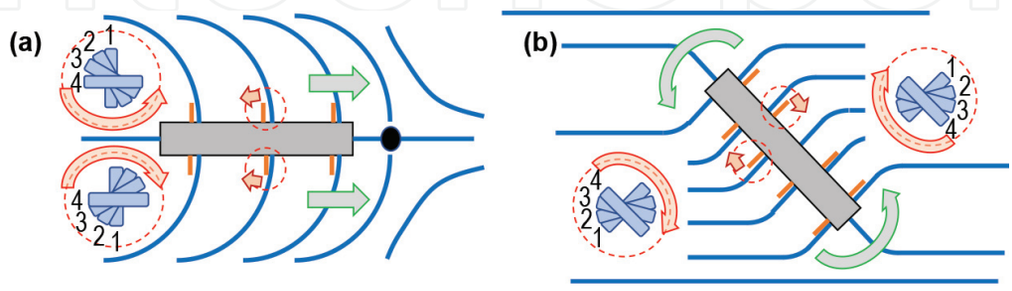

Figure 28. Cartoons showing the mechanisms of (a) the lateral motion and (b) the seesaw motion of microrods. Arrows indicate the bending direction in the *cis* state of azo groups [17]. The numbers from 1 to 4 in small blue rods show the rotation sequence of the directors in the vicinity of the microrods. Green arrows indicate the motion of the microrods by the torques exerted by the director rotations (red arrows) [17]. Copyright 2015, National Academy of Science.

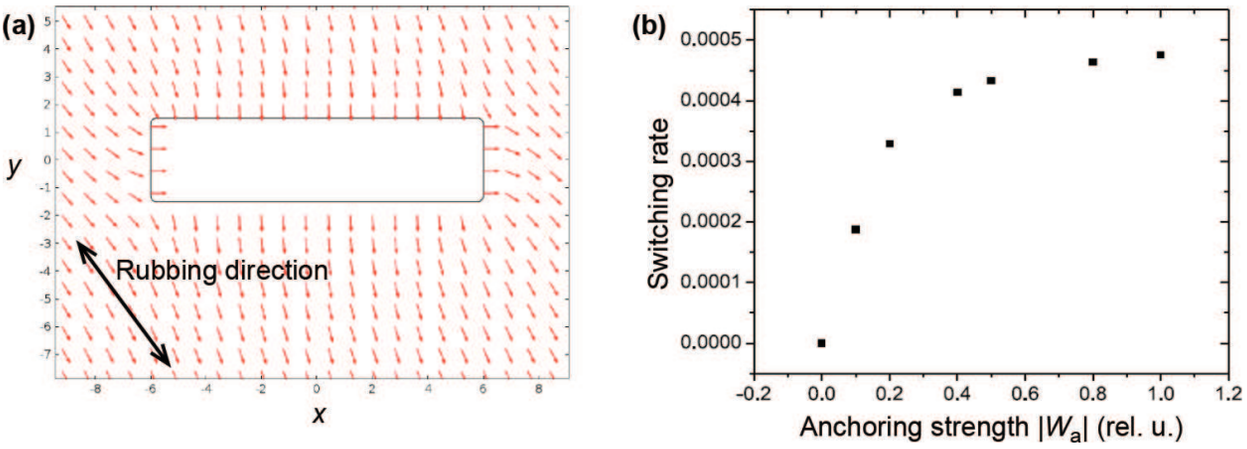

Figure 29. Simulation results of (a) a director map and (b) a switching rate as a function of anchoring strength. Since the anchoring strength is equivalent to the ratio of UV and VIS light intensities (see Section 7), (b) can be compared with **Figure 6–14(b)** under a constant VIS intensity with a sufficient agreement (SI in [17]).

where γ is a rotational viscosity coefficient. The switching behavior can be obtained by solving

$$\mathbf{n}\cdot\Delta u = \frac{W_a}{K}\sin\{2(u-u_0)\} \tag{5}$$

under an initial and boundary conditions. Here u_0 is the azimuthal angle of the director at the boundary. The results are shown in **Figure 29**; (a) the initial state of the director field and (b) switching rate (inverse switching speed) as a function of the absolute value of the anchoring strength. **Figure 29(b)** corresponds to **Figure 27(b)**, since the anchoring strength is directly related to the UV light intensity under a certain VIS light intensity (see Section 7).

7. Controlling surface anchoring strength

As mentioned in Section 6.4, the orientation change due to the command surface is considered to be the result of the change in the anchoring strength W_a depending on n_t and n_c ratio. Here we describe more quantitative discussion together with the experimental results of W_a as a function of the ratio of UV and VIS light intensities [19]. In the precedent section, we only paid attention to the UV light intensity I_{UV}, but neglected the effect of VIS intensity I_{VIS}. Careful experiment, however, indicates that the surface anchoring condition is governed both by I_{UV} and I_{VIS}, as shown in **Figure 30**; homeotropic alignment is realized when I_{VIS} is strong and I_{UV} is week, and planar alignment is realized in the opposite situation. The order parameter obtained by anisotropic infrared absorption of the C ≡ N peak shows the variation from positive to negative with increasing I_{UV} under a certain I_{VIS} light irradiation [19].

The anchoring strength W_a can be obtained by determining an extrapolation length ξ using the Freedericksz transition method in appropriate cell geometries.

$$\xi = K/W_a. \tag{6}$$

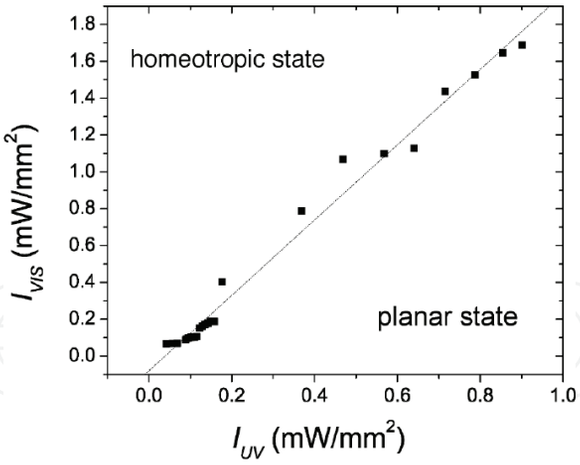

Figure 30. Homeotropic and planar states realized under different UV and VIS light intensities [19]. Copyright 2017, Royal Society of Chemistry.

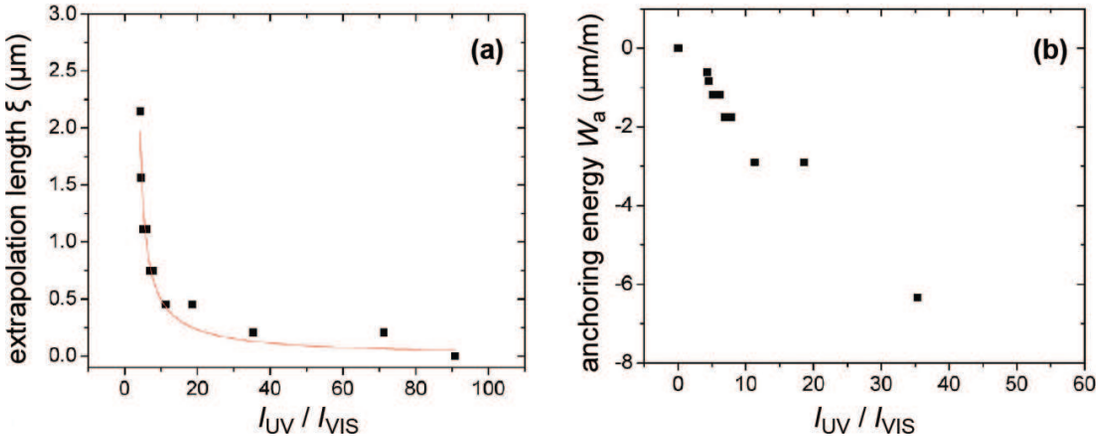

Figure 31. (a) Extrapolation length as a function of I_{UV}/I_{VIS}. (b) Anchoring energy as a function of I_{UV}/I_{VIS} [19]. Copyright 2017, Royal Society of Chemistry.

Here K is the elastic constant corresponding to the electric-induced director deformation. The obtained ξ and W_a are shown in **Figure 31**.

For the analysis of Eq. (1), we neglected the third term, that is, thermal relaxation from *cis*-to-*trans*, but properly took into account the second term, then we obtain the I_{UV}/I_{VIS}-dependent stationary values of *cis* and *trans* isomer populations, n_{c0} and n_{t0}, respectively:

$$n_{c0} = \frac{k_{tc} I_{UV}}{k_{tc} I_{UV} + k_{ct} I_{VIS}} n, \tag{7}$$

$$n_{t0} = \frac{k_{ct} I_{VIS}}{k_{tc} I_{UV} + k_{ct} I_{VIS}} n. \tag{8}$$

Considering that W_a is $+\infty$ and $-\infty$, when all azodendrimers are *trans* and *cis*, respectively, and assuming $W_a = 0$, when $n_t = n_c$, we can empirically write W_a as.

$$W_a = \kappa n \frac{n_t - n_c}{n_t n_c}, \tag{9}$$

where κ is a scaling factor. Using Eqs. (6)–(9), we obtain

$$W_a = \kappa \frac{(k_{ct} I_{VIS})^2 - (k_{tc} I_{UV})^2}{k_{ct} k_{tc} I_{VIS} I_{UV}} = \kappa \left(\frac{1}{\eta} - \eta \right) \tag{10}$$

and

$$\xi = \frac{K}{\kappa} \frac{\eta}{1 - \eta^2} \tag{11}$$

with $\eta = k_{tc} I_{UV} / k_{ct} I_{VIS}$. Since η is directly related to the experimental parameter I_{UV}/I_{VIS}, ξ vs. I_{UV}/I_{VIS} in **Figure 31** can be fitted by Eq. (11), as shown by a solid curve in **Figure 31(a)**. Thus, the director switching by photo-isomerization of azo molecules at surfaces is ascribed to the change of the anchoring strength at surfaces.

8. Summary

We introduced various functions given by azodendrimers. First, we summarized dendrimer molecules with mesogenic groups synthesized and their mesogenic phase sequences. Some of them have a strong tendency to align themselves to homeotropic orientation. As a function for static use, we described the use for LC display applications. Spontaneous homeotropic orientation is achieved just by doping LCs with a small amount of dendrimers without pre-surface treatment. This technique can be used not only for the VA mode but also for the IPS mode, if azo linkages are introduced to the dendrimers and photo treatment is applied using linear polarized light. We can find much more functions, if dendrimers are substituted at their tail ends by azo groups. The property of spontaneous adsorption of dendrimers onto a variety of surfaces and interfaces is very important, as exemplified in LC colloidal systems and LC systems with micro inclusions, which are the main topics of this review. Because of photo-induced *trans-cis* isomerization, the azodendrimers act as a command surface, which enables us to control LC orientation. Azodendrimers can be attached to form layers at a variety of surfaces and interfaces, that is, glass substrates, LC droplets in polymers, and surfaces of microparticles in LCs. Photo-controlled *trans*- and *cis*-forms, respectively, provide homeotropic and planar orientations of LCs. The photo-irradiation triggers azodendrimers transport (dewetting) and orientation changes, resulting in various changes; macroscopically physical properties such as thermal transport, microscopically orientational defect structure changes, and even dynamics of inclusions in LCs.

Acknowledgements

This chapter provides a review of our previous works related to physical and chemical measurements using azodendrimers. We acknowledge all coauthors particularly Prof. K. Yonetake, Prof. A. Eremin, and Dr. F. Araoka for their collaboration.

Author details

Hideo Takezoe[1] and Osamu Haba[2]*

*Address all correspondence to: haba@yz.yamagata-u.ac.jp

1 Toyota Physical and Chemical Research Institute, Nagakute, Aichi, Japan

2 Department of Organic Materials Science, Yamagata University, Yamagata, Japan

References

[1] (a) Yu Y, Nakano M, Ikeda T. Photomechanics: Directed bending of a polymer film by light. Nature. 2003;**425**:145-145. (b) Yu H, Ikeda T. Photocontrollable liquid-crystalline actuators. Advanced Materials. 2011;**23**:2149-2180

[2] Ichimura K, Suzuki Y, Seki T, Hosoki A, Aoki K. Reversible change in alignment mode of nematic liquid crystals regulated photochemically by command surfaces modified with an azobenzene monolayer. Langmuir. 1988;**4**:1214-1216

[3] Gibbons WM, Shannon PJ, Sun S-T, Swetlin BJ. Surface-mediated alignment of nematic liquid crystals with polarized laser light. Nature. 1991;**351**:49-50

[4] (a) Ichimura K. Photoalignment of liquid-crystal systems. Chemical Reviews. 2000;**100**: 1847-1873. (b) Natansohn A. Photoinduced motions in azo-containing polymers. Chemical Reviews. 2002;**102**:4139-4175. (c) Yu H. Recent advances in photoresponsive liquid-crystalline polymers containing azobenzene chromophores. Journal of Materials Chemistry C. 2014;**2**:3047-3054. (d) Seki T. Light-directed alignment, surface morphing and related processes: Recent trends. Journal of Materials Chemistry C. 2016;**4**:7895-7910

[5] Newkome GR, Moorefield C, Vögtle F. Dendritic Molecules: Concepts, syntheses, perspectives. VCH: Weinheim; 1996

[6] Archut A, Vogtle F, De Cola L, Azzellini GC, Balzani V, Ramanujam PS, Berg RH. Azobenzene-functionalized cascade molecules: Photoswitchable supramolecular systems. Chemistry—A European Journal. 1998;**4**:699-706

[7] Kim JM, Shin HK, Park E, Kim CK, Kwon S-S. The study on the optical characteristics of G4-48 azodendrimer by Langmuir-Blodgett method. Molecular Crystals and Liquid Crystals. 2010;**377**:197-200

[8] Gopalan P, Katz HE, McGee DJ, Erben C, Zielinski T, Bousquet D, Muller D, Grazul J, Olsson Y. Star-shaped azo-based dipolar chromophores: Design, synthesis, matrix compatibility, and electro-optic activity. Journal of the American Chemical Society. 2004;**126**:1741-1747

[9] Li X, Lu X, Lu Q, Yan D. Photoorientation of liquid crystalline azodendrimer by nanosecond pulsed laser for liquid crystal alignment. Macromolecules. 2007;**40**:3306-3312

[10] del J, Tejedor RM, Shinelatto LS, Sanchez C, Pinol M, Oriol L. Photocontrol of the Supramolecular chirality imposed by stereocenters in liquid crystalline azodendrimers. Chemistry of Materials. 2010;**22**:1714-1723

[11] (a) Lin W, Cui Y, Gao J, Yu J, Liang T, Qian G. Six-branched chromophores with isolation groups: Synthesis and enhanced optical nonlinearilty. Journal of Materials Chemistry. 2012;**22**:9202-9208. (b) Yu Y, Cui Y, Yang Y, Qian G. Design and preparation of hybrid films containing three-branched chromophores for nonlinear optical applications. RSC Advances. 2016;**6**:81969-81975

[12] (a) Kim Y-H. Lyotropic liquid crystalline hyperbranched aromatic polyamides. Journal of the American Chemical Society. 1992;**114**:4947-4948. (b) Percec V, Chu P, Ungar G, Zhou J. Rational design of the first nonspherical dendrimer which displays calamitic nematic and smectic thermotropic liquid. Journal of the American Chemical Society. 1995;**117**:11441-11454. (c) Lorenz K, Holter D, Stuhn B, Mulhaupt R, Frey H. A mesogen-functionized carbosilane dendrimer: A dendritic liquid crystalline polymer. Advanced Materials. 1996;**8**:414-416. (d) Ponomarenko SA, Boiko NI, Shibaev VP, Richardson RM, Whitehouse IJ, Rebrov EA, Muzafarov AM. Carbosilane liquid crystalline dendrimers: From molecular architecture to supramolecular nanostructures. Macromolecules. 2000;**33**:5549-5558

[13] Yonetake K, Masuko M, Morishita T, Suzuki K, Ueda M, Nagahata R. Poly(propyleneimine) dendrimers peripherally modified with mesogens. Macromolecules. 1999;**32**: 6578-6586

[14] (a) Haba O, Okuyama K, Osawa H, Yonetake K. Structures and properties of dendrimers having peripheral 2,3-difluorobiphenyl mesogenic units: Effects of dendrimer generation. Liquid Crystals. 2005;**32**:633-642. (b) Haba O, Hiratsuka D, Shiraiwa T, Koda T, Yonetake K, Momoi Y, Furuta K. Synthesis and characterization of polypropyleneimine dendrimers having peripheral mesogenic groups: Homeotropic orientation and mesogen structure. Molecular Crystals and Liquid Crystals. 2013;**574**:84-95

[15] Li W, Dohi T, Hara M, Nagano S, Haba O, Yonetake K, Seki T. Phototriggered mass migration consorted with surface dewetting in thin films of a liquid crystalline azobenzene-containing dendrimer. Macromolecules. 2012;**45**:6618-6627

[16] Private communications by S. Aya (Riken, Japan) and by C. Park (Univ. Colorado, USA)

[17] Eremin A, Hirankittiwong P, Chattham N, Nadashi H, Stannarius R, Limtrakul J, Haba O, Yonetake K, Takezoe H. Optically driven translational and rotational motions of microrod particles in a nematic liquid crystal. Proceedings of the National Academy of Sciences. 2015;**112**:1716-1720

[18] Haba O, Hiratsuka D, Shiraiwa T, Funakoshi N, Awano H, Koda T, Takahashi T, Yonetake K, Kwak M, Momoi Y, Kim N, Hong S, Kong D, Choi Y. Homeotropic orientation of nematic liquid crystals induced by dissolving polyprophyleneimine dendrimer having peripheral mesogens. Optical Materials Express. 2014;**4**:934-943

[19] Nadasi H, Stannarius R, Eremin A, Ito A, Ishikawa K, Haba O, Yonetake K, Takezoe H, Araoka F. Photomanipulation of the anchoring strength using a spontaneously adsorbed layer of azodendrimers. Physical Chemistry Chemical Physics. 2017;**19**:7597-7606

[20] Momoi Y, Furuta K, Kwak M, Koda T, Haba O, Yonetkae K. Surface analysis of polyimide-less LC alignment by dissolving dendrimer, abstract of IDW'11:1545-1548

[21] Sakuma T, Funakoshi N, Takahashi Y, Uchida M, Koda T, Haba O, Yonetake K, Kwak M, Momoi Y, Jeon J, An S, Xhoi D, Kang D, Choi Y, Jeon S. Polyimide-less alignment by dendrimers dissolved in liquid crystal, IDW/AD'12:1595-1598

[22] Lee G, Araoka F, Ishikawa K, Momoi Y, Haba O, Yonetake K, Takezoe H. Photo-induced ordering transition in microdroplets of liquid crystals with azodendrimer. Particle and Particle Systems Characterization. 2013;**30**:847-852

[23] Momoi Y, Kwak M, Choi D, Choi Y, Jeong K, Koda T, Haba O, Yonetake K. Polimide-free LCD by dissolving dendrimers. Journal of the Society for Information Display. 2012;**20**:486-492

[24] Haba O, Yonetake K. Application of dendrimers to liquid crystal displays. Journal of the Japan Society of Colour Material (in Japanese). 2013;**86**:433-438

[25] Haba O, Itabashi H, Sato S, Machida K, Koda T, Yonetake K, Kwak M, Momoi Y, Kim N, Hong S, Kang D, Choi Y. UV-induced stable planar alignment of nematic LCs using a polypropyleneimine dendrimer having a mesogen consisting of cinnamate and azobenzene moieties. Molecular Crystals and Liquid Crystals. 2015;**610**:201-209

[26] Ryu M, Takezoe H, Haba O, Yonetake K, Morikawa J. Photo-controllable thermal diffusivity and thermal conductivity driven by the orientation change of nematic liquid crystal with azodendrimers. Applied Physics Letters. 2015;**107**:221901-1-221901-4

[27] Morikawa J, Hashimoto T. Thermal diffusivity of aromatic polyimide thin films by temperature wave analysis. Journal of Applied Physics. 2009;**105**:113506-1-113506-9

[28] (a) Rochon P, Batalla E, Natansohn A. Optically induced surface gratings on azoaromatic polymer films. Applied Physics Letters. 1995;**66**:136-138. (b) Kim DY, Tripathy SK, Li L, Kumar J. Laser-induced holographic surface relief gratings on nonlinear optical polymer films. Applied Physics Letters. 1995;**66**:1166-1168

[29] (a) Nakano H, Takahashi T, Kadota T, Shirota Y. Formation of a surface relief grating using a novel azobenzene-based photochromic amorphous molecular material. Advanced Materials. 2002;**14**:1157-1160. (b) Ishow E, Lebon B, He Y, Wang X, Bouteiller L, Galmeche L, Nakatani K. Structural and photoisomerization cross studies of polar photochromic monomeric glasses forming surface relief gratings. Chemistry of Materials. 2006;**18**:1261-1267

[30] Galgano JJ, Karunatilaka C, Rethwisch DG, Tivanski AV. Atomic force microscopy study of photoreversible nanoscale surface relief grating patterns on side chain dendritic polyester thin films. Colloids and Surfaces A. 2010;**360**:167-174

[31] (a) Ubukata T Seki T, Ichimura K. Surface relief gratings in host-guest supramolecular materials. Advanced Materials. 2000;**12**:1675-1678. (b) Isayama J, Nagano S, Seki T. Phototriggered mass migrating motions in liquid crystalline azobenzene polymer films with systematically varied thermal properties. Macromolecules. 2010;**43**:4105-4112

[32] Ikeda T, Aya S, Araoka F, Ishikawa K, Haba O, Yonetake K, Momoi Y, Takezoe H. Novel bistable device using anchoring transition and command surface. Applied Physics Express. 2013;**6**:061701-1-061701-3

[33] Dhara S, Kim JK, Jeong SM, Kogo R, Araoka F, Ishikawa K, Takezoe H. Anchoring transition of transversely polar liquid-crystal molecules on perfluoropolymer surfaces. Physical Review E. 2009;**79**:060701(R)-1-060701(R)-4

[34] (a) Kim JK, Araoka F, Jeong SM, Dhara S, Ishikawa K, Takezoe H. Bistable device using anchoring transition of nematic liquid crystals. Applied Physics Letters. 2009;**95**:063505-1-063505-3. (b) Jampani VSR, Skarabot M, Takezoe H, Musevic I, Dhara S. Laser-driven microflow-induced bistable orientation of a nematic liquid crystal in perfluoropolymer-treated unrubbed cells. Optics Express. 2013;**21**:724-729

[35] (a) Shyang L, Cheng Y, Zhao Y. Emerging droplet microfluidics. Chemical Reviews. 2017;**117**:7964-8040. (b) Wang X, Bukusoglu E, Abbott NI. A practical guide to the preparation of liquid crystal-templated microparticles. Chemistry of Materials. 2017;**29**:53-61. (c) Sengpta A. Herminghaus S, Bahr C. Liquid crystal microfluidics: Surface, elastic and viscous interactions. Liquid Crystals Reviews. 2014;**2**:73-110

[36] (a) Press MJ, Arrott AS. Theory and experiments on configurations with cylindrical symmetry in liquid-crystal droplets. Physical Review Letters. 1974;**33**:403-406. (b) Stark H. Physics of colloidal dispersions in nematic liquid crystals. Physics Reports. 2001;**351**:387-474. (c) Blanc C, Coursault D, Lacaze E. Ordering nano- and microparticles assemblies with liquid crystals. Liquid Crystals Reviews. 2013;**1**:83-109. (d) Orlova T, Asshoff SJ, Yamaguchi T, Katsonis N, Brasselet E. Creation and manipulation of topological states in chiral nematic microspheres. Nature Communications. 2015;**6**:7603-1-7603-9

[37] (a) Yamamoto T, Tabe Y, Yokoyama H. Photochemical transformation of topological defects formed around colloidal droplets dispersed in azobenzene-containing liquid crystals. Colloids and Surfaces A: Physicochemical and Engineering Aspects. 2009;**334**:155-159. (b) Yamamoto T, Tabe Y, Yokoyama H. Photochemical manipulation of topological defects in liquid-crystal emulsions doped with azobenzene derivatives. Thin Solid Films. 2006;**509**:81-84

[38] Takezoe H, Eremin A. Bend-shaped Liquid Crystals–Structures and Physical Properties. CRC Press; Boca Raton. 2017

[39] (a) Aya S, Obara H, Pociecha D, Araoka F, Okano K, Ishikawa K, Gorecka E, Yamashita T, Takezoe H. Highly elastic liquid crystal with bend elastic constant of sub-nN mediated by the resident molecular assemblies. Advanced Materials. 2014;**26**:1918-1922. (b) Aya S, Ogino S, Hayashi Y, Okano K, Pociecha D, Le KV, Araoka F, Kawauchi S, Gorecka E,

Vaupotic N, Takezoe H, Ishikawa K. Structure-sensitive bend elastic constants between piconewton and sub-nanonewton in diphenylacetylene-core-based liquid crystals. Physical Review E. 2014;**90**:042506-1-042506-6

[40] (a) Kleman M, Lavrentovich OD. Topological point defects in nematic liquid crystals. Philosophical Magazine. 2006;**86**:4117-4137. (b) Lavrentovich OD. In: Arodz H, editor. Defects in liquid crystals: Surface and interfacial anchoring effects, in patterns of symmetry breaking. Netherland: Kluwer Academic Pub.; 2003

[41] (a) Poulin P, Cabuil V, Weitz DA. Direct measurement of colloidal forces in an anisotropic solvent. Physical Review Letters. 1997;**79**:4862-4865. (b) Poulin P, Stark H, Lubensky TC, Weitz DA. Novel colloidal interactions in anisotropicfluids. Science. 1997;**275**:1770-1773

[42] Pishnyak OP, Shiyanovskii SV, Lavrentovich OD. Aggregation of colloidal particles in a non-equilibrium backflow induced by electrically-driven reorientation of the nematic liquid crystal. Journal of Molecular Liquids. 2011;**164**:132-142

[43] Smalyukh II, Kaputa DS, Kachynski AV, Kuzmin AN, Prasad PN. Optical trapping of director structures and defects in liquid crystals using laser tweezers. Optics Express. 2007;**15**:4359-4371

[44] Skarabot M, Lokar Z, Musevic I. Transport of particles by a thermally induced gradient of the order parameter in nematic liquid crystals. Physical Review E. 2013;**87**:062501-1-062501-6

[45] Hirankittiwong P, Chattham N, Limtrakul J, Haba O, Yonetake K, Eremin A, Stannarius R, Takezoe H. Optical manipulation of the nematic director field around microspheres covered with an azo-dendrimer monolayer. Optics Express. 2014;**22**:20087-20093

[46] (a) Lapointe C, Hultgren A, Silevitch DM, Felton EJ, Reich DH, Leheny RL. Elastic torque and the levitation of metal wires by a nematic liquid crystal. Science. 2004;**303**:652-655. (b) Tkalec U, Skarabot M, Musevic I. Interactions of micro-rods in a thin layer of a nematic liquid crystal. Soft Matter. 2008;**4**:2402-2409. (c) Juhl AT, Yang D-K, Tondiglia VP, Natarajan LV, White TJ, Bunning TJ. Ordering of glass rods innematic and cholesteric liquid crystals. Optical Materials Express. 2011;**1**:1536-1547. (d) Gharbi MA, Cavallaro Jr, M, Wu G, Beller DA, Kamien RD, Yang S, Stebe KJ. Micro-bullet assembly: Interactions of oriented dipoles in confined nematic liquid crystal. Liquid Crystals. 2013;**40**:1619-1627. (e) Mundoor H, Senyuk B, Smalyukh II. Triclinic nematic colloidal crystals from competing elastic and electrostatic interactions. Science. 2016;**352**:69-73